

Deciphering the metamorphic evolution of the Pulo do Lobo metasedimentary domain (SW Iberian Variscides)

Irene Pérez-Cáceres^{1,2}, David Jesús Martínez Poyatos¹, Olivier Vidal³, Olivier Beyssac⁴,
Fernando Nieto⁵, José Fernando Simancas¹, Antonio Azor¹ and Franck Bourdelle⁶

¹ Departamento de Geodinámica, Facultad de Ciencias, Universidad de Granada, Campus de Fuentenueva s/n, 18071 Granada, Spain.

² Instituto de Ciencias de la Tierra Jaume Almera ICTJA-CSIC, C/Lluís Solé i Sabarís s/n, 08028, Barcelona, Spain.

³ Institut de Sciences de la Terre (ISTerre), CNRS-University of Grenoble 1, 1381 rue de la Piscine, 38041 Grenoble, France.

⁴ Institut de Physique des Matériaux et de Cosmochimie (IMPMC), CNRS-Sorbonne Université, Case Courrier 115, 4 place Jussieu, 75005 Paris, France.

⁵ Departamento de Mineralogía y Petrología, IACT, Facultad de Ciencias, Universidad de Granada-CSIC, Campus de Fuentenueva s/n, 18071 Granada, Spain.

⁶ Laboratoire Génie Civil et géo-Environnement (LGCgE), Université de Lille, Bât. SN5, Cité Scientifique, 59655 Villeneuve d'Ascq, France.

Correspondence to: Irene Pérez-Cáceres (perezcaceres@ugr.es)

Abstract

The Pulo do Lobo domain is one of the units exposed within the orogenic suture zone between the Ossa-Morena and the South Portuguese zones in the SW Iberian Variscides. This metasedimentary unit has been classically interpreted as a Rheic subduction-related accretionary prism formed during pre-Carboniferous convergence and eventual collision between the South Portuguese Zone (part of Avalonia) and the Ossa-Morena Zone (peri-Gondwanan terrane). Discrete mafic intrusions also occur within the dominant Pulo do Lobo metapelites, related to an intraorogenic Mississippian transtensional and magmatic event that had a significant thermal input. Three different approaches have been applied to the Devonian/Carboniferous phyllites and slates of the Pulo do Lobo domain in order to study their poorly known low-grade metamorphic evolution. X-Ray diffraction (XRD) was used to identify the mineralogy and measure crystallographic parameters (illite “crystallinity” and K-white mica *b*-cell dimension). Compositional maps of selected samples were obtained from electron probe microanalysis, which allowed processing with XmapTools software, and

chlorite semi-empirical and thermodynamic geothermometry was performed. Thermometry based on Raman spectroscopy of carbonaceous material (RSCM) was used to obtain peak temperatures.

The microstructural study shows the existence of two phyllosilicate growth events in the chlorite zone, the main one (M_1) related to the development of a Devonian foliation S_1 , and a minor one (M_2) associated with a crenulation cleavage (S_2) developed in middle/upper Carboniferous time. M_1 entered well into epizone (greenschist facies) conditions. M_2 conditions were at lower temperature, reaching the anchizone/epizone boundary. These data accord well with the angular unconformity that separates the Devonian and Carboniferous formations of the Pulo do Lobo domain. The varied results obtained by the different approaches followed, combined with microstructural analysis, provide different snapshots of the metamorphic history. Thus, RSCM temperatures are higher in comparison with the other methods applied, which is interpreted to reflect a faster reequilibration during the short-lived thermal Mississippian event. Regarding the metamorphic pressure, the data are very homogeneous: very low celadonite content (0-10 %) in muscovite (and low values of K-white mica *b*-cell dimension (8.995 Å mean value), indicating a low pressure/temperature gradient, which is unexpected in a subduction-related accretionary prism.

Keywords

Pulo do Lobo metapelites

Low-pressure gradient

Illite “crystallinity”

Chlorite geothermometry

Raman spectroscopy of carbonaceous material

Highlights

A multidisciplinary approach has been applied to study the metamorphism of the Pulo do Lobo metapelites.

Devonian metamorphism entered epizone conditions.

Carboniferous metamorphism reached the anchizone/epizone boundary.

The inferred low-pressure gradient is incompatible with a subduction-related accretionary prism.

1. Introduction

The determination of temperature and pressure conditions reached by the low-grade metasedimentary units stacked hinterlands of orogens constrains their tectonometamorphic evolution (e.g., Goffé and Velde, 1984; Franceschelli et al., 1986; Ernst, 1988; Gutiérrez-Alonso and Nieto, 1996; Frey and Robinson, 1999; Bousquet et al., 2008; Lanari et al., 2012). The various results derived from the application of diverse geothermometric and/or geobarometric methods may also allow the identification and characterization of superposed tectonometamorphic events, thus improving the knowledge of the P-T paths and their tectonic significance (e.g., Brown, 1993; Crouzet et al., 2007; Ali, 2010; Lanari et al., 2012; Airaghi et al., 2017).

The metamorphism of the Iberian Variscides has been mostly studied on high grade metamorphosed rocks in order to characterize and obtain the P-T-t paths of suture-related units (e.g., Gil Ibarguchi et al., 1990; Abalos et al., 1991; Escuder Viruete et al., 1994; Barbero, 1995; Arenas et al., 1997; Fonseca et al., 1999; López-Carmona et al., 2013; Martínez Catalán et al., 2014). The low- to very low-grade units have been also studied (e.g., Martínez Catalán, 1985; Bastida et al., 1986, 2002; López Munguira et al., 1991; Gutiérrez-Alonso and Nieto, 1996; Abad et al., 2001, 2002, 2003a; Martínez Poyatos et al., 2001; Nieto et al., 2005; Vázquez et al., 2007), despite the scarcity of appropriate robust methodologies to apply in these kind of rocks. Obtaining new results from the low-grade rocks of the Pulo do Lobo domain, a suture-related low-grade unit in SW Iberia, is of prime importance in order to understand its significance and tectonometamorphic evolution, whose interpretations have been cause of discrepancies, and to reconstruct the overall history of the SW Iberian Variscides.

In this work, three different methodologies are applied to a number of samples of the Pulo do Lobo domain (Fig. 1): (i) X-Ray Diffraction (XRD) in order to identify minerals not easily recognizable with optical microscopy (fine-grained muscovite, paragonite, mixed-layer phyllosilicates, etc.) and obtain thermobarometric information via the measurement of crystallographic parameters (illite “crystallinity” and *b*-cell dimension); (ii) Compositional maps derived from electron probe microanalysis (EPMA), which enable the recognition of different tectonometamorphic events by combining mineral composition and microtextural features (e.g., Airaghi et al., 2017), as well as the application of geothermobarometers based on chlorite and K-white mica compositions; and (iii) Raman spectroscopy of carbonaceous material (RSCM) to estimate peak temperatures using an adapted thermometric calibration. The results obtained enables discussing the tectonometamorphic evolution of the Pulo do Lobo domain. Moreover, the comparison of the different approaches tests their reliability and sensitivity to characterize different geological processes.

2. Geological setting

The SW Iberian Variscides resulted from the Devonian-Carboniferous left-lateral oblique collision of three different terranes: the Central Iberian Zone (CIZ), the Ossa-Morena Zone (OMZ) and the South Portuguese Zone (SPZ) (Fig. 1a), and the boundaries between these terranes are considered as orogenic sutures (e.g., Quesada, 1991; Pérez-Estaún and Bea, 2004;

Pérez-Cáceres et al., 2016). Besides the dominant left-lateral shortening kinematics, SW Iberia also attests Mississippian synorogenic sedimentary basins, widespread mafic magmatism and high-temperature metamorphic areas, which together suggest an intraorogenic transtensional stage (Simancas et al., 2003, 2006; Pereira et al., 2012; Azor et al., 2019).

The OMZ is commonly interpreted as a fragment of continental crust that drifted from the CIZ (i.e., north Gondwana) in early Paleozoic times (Matte, 2001). The OMZ/CIZ suture (Badajoz-Córdoba Shear Zone) includes early Paleozoic amphibolites with oceanic affinity, eclogite relicts and intense high- to low-grade left-lateral shear deformation (Burg et al., 1981; Abalos et al., 1991; Quesada, 1991; Azor et al., 1994; Ordóñez-Casado, 1998; López Sánchez-Vizcaíno et al., 2003; Pereira et al., 2010). Ediacaran to Carboniferous sedimentary successions with an angular unconformity at the base of the Lower Carboniferous characterize the OMZ. Low-grade regional metamorphism dominates the OMZ, though there are areas of high-temperature / low-pressure metamorphism associated with Early Carboniferous magmatism (e.g. Bard, 1977; Crespo-Blanc, 1991; Díaz Azpiroz et al., 2006; Pereira et al., 2009).

The SPZ is a continental piece considered as a fragment of Avalonia, and thus the OMZ/SPZ boundary is usually interpreted as the Rheic Ocean suture (Crespo-Blanc and Orozco; 1988; Eden and Andrews, 1990; Silva et al., 1990; Quesada et al., 1994; Braid et al., 2011; Pérez-Cáceres et al., 2015, 2017). This boundary is delineated by the Beja-Acebuches Amphibolites (Fig. 1b), a narrow strip of metamafic rocks that resembles a dismembered ophiolitic succession (from greenschists to metagabbros and locally ultramafic rocks) (e.g., Bard, 1977; Crespo-Blanc, 1991; Quesada et al., 1994). This unit was interpreted as a Rheic ophiolite (Munhá et al., 1986; Crespo-Blanc, 1991; Fonseca and Ribeiro, 1993; Quesada et al., 1994; Castro et al., 1996). This idea was reconsidered based on the Mississippian age of the mafic protholits (≈ 340 Ma; Azor et al., 2008) and is more likely evidence of the early Carboniferous intraorogenic, lithospheric-scale transtensional and magmatic episode that obscures the previous suture-related features of the OMZ/SPZ boundary (Pérez-Cáceres et al., 2015 and references therein). Nevertheless, there is also the alternative explanation that the OMZ/SPZ boundary was a protected tract of Rheic oceanic lithosphere that did not close until Carboniferous time (Murphy et al., 2016; Braid et al., 2018; Quesada et al., 2019). The rocks of the Beja-Acebuches Amphibolites were affected by a left-lateral ductile shearing which occurred at granulite to greenschist facies conditions, though amphibolite facies conditions were dominant (e.g., Quesada et al., 1994; Castro et al., 1996; Castro et al., 1999; Díaz Azpiroz et al., 2006). This metamorphism has been dated at 345-330 Ma (Dallmeyer et al., 1993; Castro et al., 1999), thus suggesting that it started very shortly after the magmatic emplacement.

North of the Beja-Acebuches Amphibolites, the allochthonous Cubito-Moura unit might be the only vestige of the Rheic Ocean suture (Fonseca et al., 1999; Araújo et al., 2005; Pérez-Cáceres et al., 2015). This unit was emplaced onto the southern OMZ border (Fig. 1b) with a left-lateral top-to-the-ENE kinematics (Ponce et al., 2012). It contains Ediacaran-Lower Paleozoic metasedimentary rocks and Ordovician MORB-featured mafic rocks (≈ 480 Ma; Pedro et al., 2010) transformed into high-pressure blueschists and eclogites at ≈ 370 Ma (Moita et al., 2005). The high-pressure metamorphism has also been studied by using white

mica and chlorite (and chloritoid pseudomorphs) mineral equilibria (Booth-Rea et al., 2006; Ponce et al., 2012; Rubio Pascual et al., 2013), yielding peak conditions of 1 GPa at 450 °C.

South of the Beja-Acebuches Amphibolites, low- to very low-grade successions crop out: Devonian siliciclastics, earliest Carboniferous volcano-sedimentary rocks, and a south-migrating Carboniferous flysch (e.g., Oliveira, 1990). These rocks are usually grouped into two geological domains: the Pulo do Lobo domain to the north, and the SPZ s. str. to the south (Fig. 1a, b). The deformation in the SPZ consists of a south- to southwest-vergent fold and thrust belt with decreasing strain intensity and age southwards (Oliveira, 1990; Simancas et al., 2004). The metamorphic grade also decreases southwards, from epizone to diagenetic, through the SPZ (Munhá, 1990; Abad et al., 2001). The Pulo do Lobo domain, which has been traditionally considered as a suture-related unit (see below) is the focus of this work.

2.1. Pulo do Lobo domain

The Pulo do Lobo domain constitutes a polydeformed structure affecting low-grade Devonian-Carboniferous sedimentary formations. These formations are, from bottom to top (Fig. 1b-c):

(i) The Pulo do Lobo Formation (s. str.), which is constituted by a succession of satiny black to grey phyllites and fine-grained schists with minor intercalations of quartz sandstones (Fig. 2a). The presence of abundant segregated quartz veins (pre- to post-folding) is common. The palynological content suggests a middle Frasnian age (Pereira et al., 2018).

(ii) The Ribeira de Limas Formation, which is constituted by phyllites with thin beds of quartz sandstones and arkoses (Fig. 2b). The presence of palynomorphs also suggests a middle Frasnian age for this formation (Pereira et al., 2018). The contact with the underlying Pulo do Lobo Formation is gradual, with a progressive increase of sandstones and a decrease of phyllites upwards. For that reason, we will refer to the Pulo do Lobo and Ribeira de Limas formations as the lower formations of the Pulo do Lobo domain. Furthermore, these lower formations share the same structural fabrics consisting of three fold-related foliations (Fig. 2a-b; Pérez-Cáceres et al., 2015). The first foliation of the lower formations (S_1) is preserved inside microlithons of the second foliation (S_2); usually, the angle between these two foliations is high. S_2 is the main foliation and consists in a crenulation-dissolution cleavage that commonly appears as a milimetric- to centimetric-spaced tectonic banding. This foliation is axial-planar to north-vergent folds. The third foliation (S_3) is a spaced crenulation-dissolution cleavage that typically develops a characteristic decimetric- to metric-scale tectonic banding. S_3 is associated with upright to slightly south-vergent folds.

(iii) The Santa Iria Formation, which is composed by alternating beds of slates and greywackes (Fig. 2c). The greywacke beds show normal grading and an erosive base. Paleontological and palynostratigraphic studies suggest an Upper Famennian age for this formation (Pereira et al., 2008; 2018). However, an early Carboniferous age is also plausible, since more than 90% of the palynomorphs correspond to reworked material (Lopes et al., 2014) and the younger detrital zircon population is early Carboniferous (Braid et al., 2011; Pérez-Cáceres et al., 2017; Pereira et al., 2019). The Santa Iria Formation only shows two foliations, correlative with the last two deformation phases in the lower formations.

Therefore, an unconformity between them is inferred, which is consistent with the age and flysch character of the Santa Iría Formation (Pérez-Cáceres et al., 2015). S_2 is observed as a penetrative slaty cleavage, while S_3 is a disjunctive crenulation cleavage.

According to Silva et al. (1990) and Pérez-Cáceres et al. (2015), the two main foliations (S_2 and S_3) in the Pulo do Lobo domain resulted from the middle/upper Carboniferous collision between the OMZ and SPZ. The first foliation (S_1) in the Pulo do Lobo domain might have formed during the convergence of the Rheic Ocean subduction and/or the beginning of the Variscan collision, probably at Late Devonian time.

The Pulo do Lobo domain contains some decimetric- to metric-scale lenticular bodies of MORB-featured metamafic rocks. At some outcrops, the mafic rocks are embbeded in a greenish detrital matrix, thus suggesting an olistostromic origin (the Peramora Olistostrome; Eden and Andrews, 1990). These rocks are tectonically imbricated with the phyllites of the Pulo do Lobo Formation and hence forming a tectonic *mélange* (the so-called Peramora *Mélange*; Fig. 1b-c; Eden, 1991; Dahn et al., 2014). Based on this aspect and on the supposedly Rheic Ocean derived greenschists, the Pulo do Lobo domain has been classically interpreted as a pre-collisional subduction-related accretionary prism (Eden and Andrews, 1990; Silva et al., 1990; Eden, 1991; Braid et al., 2010; Ribeiro et al., 2010; Dahn et al., 2014; Quesada et al., 2019). However, the recently obtained Mississippian U/Pb zircon ages from the metamafic rocks (Dahn et al., 2014; Pérez-Cáceres et al., 2015) make it difficult to maintain such an hypothesis. More properly, they can be interpreted as mafic intrusions/extrusions in the frame of the intraorogenic transtensional magmatic event that prevailed in SW Iberia during the Mississippian. The metamafic rocks display a foliation (equivalent to the S_2 of the enveloping metasediments) developed during loosely constrained greenschist facies metamorphism. These rocks would have been imbricated with the Pulo do Lobo metasedimentary rocks during the second deformation phase which caused S_2 (Pérez-Cáceres et al., 2015). Our multidisciplinary metamorphic study of the Pulo do Lobo metasediments provides crucial data concerning the tectonic significance of this domain.

3. Samples and analytical methods

Eighteen samples were collected from well-exposed outcrops of phyllosilicate-rich detrital rocks of the Pulo do Lobo domain along two north-south transects perpendicular to the structural trend. Five samples belong to the Santa Iría Formation (unconformable upper formation) and thirteen to the lower formations (Pulo do Lobo and Ribeira de Limas formations) (location of samples are shown in the map and cross-sections of Fig. 1b-c and the UTM coordinates are given in supplementary information). As a whole, the samples were selected in fresh outcrops, far from faults and joints, and were as homogeneous and representative as possible. Sampling strategy was to collect representative sites, both of the overall stratigraphic succession and along two transects. We also aimed to characterize the unconformity between the lower and upper formations from a metamorphic point of view, since “crystallinity” aspect to the naked eye appears to be lower in the Santa Iría Formation. Some samples from the lowermost Pulo do Lobo Formation were collected ≈ 200 m from the metabasite lenses of the Peramora *Mélange*.

Samples were examined under the optical microscope and scanning electron microscope (SEM) for overall mineralogy, deformation textures and minerals/foliations relationships using an environmental scanning electron microscope FEI model Quanta 400, operating at 15–20 keV (Centro de Instrumentación Científica-CIC, University of Granada, Spain).

3.1. X-Ray diffraction

Sample preparation and analysis by XRD were done in the laboratories of the Department of Mineralogy and Petrology of the University of Granada (Spain). After washing and cleaning of patinas and oxides, samples were crushed to a <2 mm fraction. The <2 μm fractions were separated by repeated extraction of supernatant liquid after centrifugation, according to the Stokes' law. Oriented aggregates were prepared by sedimentation on glass slides of whole-rock and <2 μm fractions (the latter aims to minimize the content of detrital micas non-re-equilibrated during very low-grade metamorphism, which are generally larger than 2 μm ; Moore and Reynolds, 1997). Samples were also treated with ethylene glycol (EGC) to identify illite/smectite or chlorite/smectite mixed-layers on the basis of their expandibility. Samples were analyzed using a PANalytical X'Pert Pro powder diffractometer equipped with an X'Celerator detector, $\text{CuK}\alpha$ radiation, operated at 45 kV and 40mA, Ni filter and 0.25° divergence slit. The resulting diffraction diagrams were examined to extract information on mineralogy based on their characteristic reflections and white mica crystal data.

The Illite “Crystallinity” index (Kübler Index; KI; Kübler, 1968) has been estimated from the measurement of the full peak-width of K-white mica at half maximum intensity (FWHM values), expressed as $\Delta^\circ 2\theta$ of the Bragg angle. Preparation of samples and experimental conditions were carried out according to IGCP 294 IC Working Group recommendations (Kisch, 1991). A step increment of 0.008° 2θ and a counting time of 52 s/step were used in the diffractometer. The KI was measured in all samples for both the 5 and 10 Å reflection peaks of K-white mica in order to identify possible effects of other overlapping phases (Nieto and Sánchez-Navas, 1994; Battaglia et al., 2004). Some XRD traces showing complex mixture of mixed-layered minerals were decomposed with the MacDiff software (Petschick, 2004). The FWHM values obtained in the laboratory (x) were transformed to Crystallinity Index Standard (CIS) values (y) using the equation $y = 0.972x + 0.1096$ ($R^2 = 0.942$), obtained from the measure in our laboratory of the international standards of Warr and Rice (1994). Finally, these values are expressed in terms of traditional KI values using the equation of Warr and Ferreiro Mähnlmann (2015; ‘CIS’ = $1.1523 \times \text{Kübler index 'Basel lab'} + 0.036$). The lower and upper boundaries of the anchizone in the KI scale are 0.42 and 0.25 ° 2θ , respectively (Warr and Ferreiro Mähnlmann, 2015). The thermal range for the anchizone is estimated in c. 200–300 °C, though the KI cannot be considered as a true geothermometer (Frey, 1987; Kisch, 1987).

The *b*-cell parameter of white mica was obtained from the (060) reflection peak measured with quartz as internal standard on polished rock-slices cut normal to the sample main foliation S_2 (Sassi and Scolari, 1974). The *b*-cell dimension of K-white mica is typically proportional to the extent of phengitic substitution and therefore is considered a proxy of the pressure conditions during its crystallization. Thus, Guidotti and Sassi (1986) have shown

that b values lower than 9.000 Å are typical of low-pressure facies conditions, while b values higher than 9.040 Å are related to relatively high-pressure facies metamorphism. Precise measurements of the basal spacing of white mica (d_{001}) have also been made, using quartz from the sample itself as internal standard. d_{001} is related to the paragonitic Na/K substitution (Guidotti et al., 1992), thereby approximately reflecting the temperature of white-mica formation (Guidotti et al., 1994).

3.2. EPMA-derived X-Ray compositional maps and chlorite thermometry

From all of the collected samples, we selected those with the larger phyllosilicate grain-size for electron probe microanalysis (EPMA). Thus, three carbon-coated polished thin-sections were studied. The selected samples (PLB-84, PLB-88 and PLB-93) belong to the lower formations of the Pulo do Lobo domain (Fig. 2d-e). The Santa Iría samples could not be studied due to the tiny grain size of the minerals (commonly less than 3 µm).

Compositional maps and accurate spot analyses were performed on a JEOL JXA-8230 EPMA at the Institut des Sciences de la Terre (ISTerre) in Grenoble (France), according to the analytical procedure proposed by De Andrade et al. (2006) and Lanari et al. (2014a). The data acquisition was made in wavelength dispersive spectrometry mode (WDS). Ten elements (Si, Ca, Al, K, Mn, Na, P, Ti, Fe and Mg) were analyzed using five WD spectrometers: TAP crystal for Si and Al, PETL for Ti and P, TAPH for Na and Mg, PETH for K and Ca, and LIFH for Mn and Fe. The standardization was made by using certified natural minerals and synthetic oxides: wollastonite (Si, Ca), corundum (Al), orthoclase (K), rhodonite (Mn), albite (Na), apatite (P), rutile (Ti), hematite (Fe), and periclase (Mg). X-Ray maps were obtained by adding successive adjacent profiles. Beam current of 100 nA and beam size spot (focused) were used. The step (pixel) size was 1 µm and the dwell time was 200-300 msec per pixel. Spot analyses were obtained along the profiles within the mapping at 15 kV accelerating voltage, 12 nA beam current and 2 µm beam size spot (focused). The on-peak counting time was 30 sec for each element and 30 sec for two background measurements at either side of each peak. ZAF correction procedure was applied. The internal standards were orthoclase and/or chromium-augite (Jarosewich et al., 1980), which were run (3 points on each standard) after each profile in order to monitor instrumental drift and estimate analytical accuracy. Drift correction was made, if necessary, using the corresponding regression equation.

The WDS X-Ray maps were then processed with XMapTools (<http://www.xmaptools.com>), a MATLAB®-based graphical user interface program to process the chemical maps, link them to thermobarometric models and estimate the pressure-temperature conditions of crystallization of minerals in metamorphic rocks (Lanari et al., 2014a). The compositional maps were standardized with the spot analyses measured along the profiles and mineral compositions were plotted into binary and ternary diagrams using the interface modules *Chem2D* and *Triplot3D*. Chemical maps of amount of tetrahedral aluminum (Al^{IV}) of chlorites were acquired, because these amounts are used in many empirical chlorite thermometers (e.g. Cathelineau and Nieva, 1985; Cathelineau, 1988). The temperature conditions were estimated for each chlorite pixel of the maps using the chlorite

thermometer of Lanari et al. (2014b), as well as the approaches of Vidal et al. (2006) and Bourdelle et al. (2013), which are summarized in the supplementary information.

In addition to the above mentioned compositional maps, white micas from seven carbon-coated thin sections of the lower formations of the Pulo do Lobo domain were analyzed before with a Jeol WDS four-spectrometer microprobe (JXA-8200 Superprobe) at the University of Huelva (Spain). A combination of silicates and oxides were used for calibration: standards used were wollastonite (Si and Ca), potassium feldspar (Al, K and Na), forsterite (Mg) and fayalite (Fe). Single point analyses were obtained with 20 nA probe current, 1-5 μm spot size and 15 kV of acceleration voltage, with 5 s counting times.

3.3. Raman Spectroscopy of carbonaceous material

Raman Spectroscopy of Carbonaceous Material (RSCM), is based on the observation that sedimentary carbonaceous material (CM) is progressively transformed into graphite at increasing temperature. Because of the irreversible character of graphitization, CM structure is not sensitive to the retrograde path during exhumation of rocks, but depends only on the maximum temperature reached during metamorphism (Beyssac et al., 2002a). Temperature was determined in the range 330-650°C with a calibration-attached accuracy of ± 50 °C due to uncertainties in the petrologic data used for the calibration (Beyssac et al., 2002a). Relative uncertainties in temperature estimates were later reduced (around 10-15 °C; Beyssac et al., 2004). For temperature below 330 °C, Lahfid et al. (2010) performed a systematic study of the evolution of the Raman spectrum of CM in low-grade metamorphic rocks in the Glarus Alps (Switzerland). They showed that the Raman spectrum of CM is slightly different from the spectrum observed at higher temperature and they established a quantitative correlation between the degree of structuration of CM and temperature.

In this work, twelve representative thin-sections previously examined by optical microscopy were selected. From these, ten samples were analyzed (according to their larger CM grain-size and content): eight samples belong to the lower Pulo do Lobo and Ribeira de Limas formations, and the other two samples belong to the Santa Iria Formation. Polished thin-sections cut perpendicularly to the S_2 foliation were analyzed at the Institut de Minéralogie, de Physique des Matériaux et de Cosmochimie at the Sorbonne University of Paris (France). We followed closely the analytical procedure described by Beyssac et al. (2002a, b; 2003; see supplementary information). More than 15 Raman spectra (Fig. 3) were obtained for each sample using a Renishaw InVIA Reflex microspectrometer equipped with a 514.5 nm Modulaser argon laser under circular polarization. The laser was focused by a DMLM Leica microscope, and laser power was set below 1 mW at the sample surface. The Rayleigh diffusion was eliminated by edge filters and the signal was dispersed using a 1800 g/mm grating and finally analyzed by a Peltier cooled RENCAM CCD detector. The recorded spectral window was large to precisely determine the background correction, from 700 to 2000 cm^{-1} in case of low-temperature samples. Before each session, the spectrometer was calibrated with a silicon standard. CM was systematically analyzed behind a transparent adjacent mineral, generally quartz or white mica grains oriented along S_1 . For a full description of the temperature calculations see the supplementary information.

4. Results

According to the petrographic study, all the samples correspond to slates or phyllites with phyllosilicates smaller than 500 μm , composed of variable quartz + K-white mica \pm chlorite \pm feldspar \pm ore and accessory minerals (Fig. 2d-f). Samples from the Santa Iría Formation have much smaller grain-size and apparently lower “crystallinity” (Fig. 2f). The first foliation S_1 is defined by the largest micas and chlorites (Fig. 2d-e), being folded by microscopic- to centimetric-scale tight folds of the second deformation phase (Fig. 2a-b, d-e). The second foliation S_2 is the main foliation at outcrop (Fig. 2a-c), but the phyllosilicates (mostly white mica) are smaller than those in S_1 . The third foliation S_3 is a fracture cleavage that does not develop phyllosilicates (Fig 2a-c).

4.1. X-Ray diffraction

The mineralogy and crystal parameters of K-white mica obtained from the 18 samples of the Pulo do Lobo domain are summarized in Table 1. The results of KI values, b -cell parameter and d_{001} analyzed in K-white mica, obtained from whole-rock and $<2\ \mu\text{m}$ fractions are very similar, which suggests that detrital micas re-equilibrated during metamorphism.

The mineralogy of the samples is relatively simple: $\text{Qz} + \text{Ms} + \text{Fsp} + \text{Chl} \pm \text{Pg} \pm \text{C/S}$. The slates of the Santa Iría Formation have quartz, muscovite and chlorite, with chlorite/smectite interlayers (C/S) in some samples. In the lower formations, besides quartz and muscovite, chlorite is present in almost all of the samples, paragonite appears in most of them, and chlorite/smectite interlayers are occasional.

KI values measured in the 10 Å peak of white mica from the $<2\ \mu\text{m}$ fraction are shown in Table 1 and Fig. 1c with a relative colour bar from orange (lower values) to green (higher values). Values of the Santa Iría samples ($n=5$) range from 0.20 to 0.26 $\Delta^\circ 2\theta$, the mean value is 0.23 (standard deviation 0.02). In the lower formations ($n=12$), KI values range from 0.17 to 0.22, the mean value is 0.19 (standard deviation 0.02). KI values measured in the 5 Å peak (not shown to avoid repetitions) are very similar to those of the 10 Å peak.

The measured b -cell parameter of white mica varies within a close range around 9 Å (8.991-9.002). Mean value is 8.995 Å (standard deviation 0.003) for the Santa Iría Formation samples, and 8.997 Å (standard deviation 0.003) for the samples of the lower formations. d_{001} values average 9.992 Å (standard deviation 0.004) and differ slightly between upper and lower formations, with higher values in the upper formation.

The results obtained through X-Ray diffraction reflect low-grade metamorphic conditions due to the KI values between 0.17-0.26 $\Delta^\circ 2\theta$. In addition, b -cell parameters are lower than 9.000 Å which show a low-pressure metamorphic gradient (low pressure/temperature metamorphic facies conditions; Guidotti and Sassi, 1986).

4.2. Compositional maps and chlorite thermometry

X-Ray maps show the distribution of major elements and allow identification of white mica, chlorite, and some albite porphyroblasts, with ilmenite and rutile as accessory minerals (Fig. 4a-b). Although quartz is abundant in all of the samples, the areas selected for detailed X-ray mapping (composed mostly by phyllosilicates) do not contain quartz (Fig. 4a-b). White mica is abundant along both S_1 and S_2 foliations (Fig. 2d-e and 4b). Chlorite is found mostly along S_1 , but is very scarce and small-sized within S_2 (Fig. 2e and 4b), with the exception of sample PLB-93 where chlorite is similar in amount in both foliation domains (Fig. 4b).

Mapped compositions of end-members of white mica and chlorite have been plotted in the ternary diagrams of Figure 5. The composition of white mica is similar in the three maps and is close to muscovite, with 25% of pyrophyllite and very minor celadonite content (0-10%; Fig. 5a). The high content of pyrophyllite (high amount of interlayer vacancies) is typical of low-pressure illitic-mica compositions. Figure 6 shows white mica compositional ratios, which can be related to P/T conditions: they present low degree of Na substitution and low phengitic component, and so are close to the muscovite end-member in composition. These results point to low-pressure conditions and agree well with XRD results: low b -cell parameter ($< 9.000 \text{ \AA}$) and high d_{001} ($> 9.985 \text{ \AA}$; Table 1).

Chlorite compositions are variable, though all of them have in common $\approx 50\%$ clinochlore + daphnite and $\approx 50\%$ amesite + sudoite (Fig. 5b). Chlorites in sample PLB-88 are low in amesite with a large variation of clinochlore + daphnite and sudoite contents. In sample PLB-84, chlorites vary in composition between amesite and sudoite indicating a variation of Al^{IV} , which implies an increase of temperature from rims to cores as shown in the chemical maps of Fig. 4c. Finally, PLB-93 chlorites are poor in sudoite and higher in Al^{IV} content, thus suggesting higher average temperatures (Vidal et al., 2006) than in PLB-84 and PLB-88. Altogether, chlorite compositional data show the presence of two end-members: sudoite-rich low-temperature (PLB-88), and amesite-rich high-temperature (PLB-93).

Maps of Al^{IV} in chlorites are displayed in Fig. 4c. Sample PLB-88 displays lower Al^{IV} content (≈ 1.1 - 1.3 apfu) than sample PLB-93 (≈ 1.3 - 1.5 apfu). In sample PLB-84, some large chlorite grains oriented along S_1 are zoned, with higher Al^{IV} content in the cores (≈ 1.4 apfu) than in the rims (≈ 1.0 apfu; see white square in Fig. 4c). According to the empirical calibration of Cathelineau (1988), Al^{IV} in chlorites increases with temperature. Thus, the Al^{IV} content in chlorites manifests different temperatures in different samples, and also varies from core to rim in singular grains.

Temperature maps have been obtained with the semi-empirical thermometer of Lanari et al. (2014b), which assumes that Fe^{2+} is the Fe total (Fig. 4d). Temperatures range between 100-200 °C in sample PLB-88, 150-350 °C in sample PLB-84, and 200-450 °C in sample PLB-93. Tiny chlorites developed along S_2 yield lower temperatures than larger and more abundant chlorites along S_1 , with the exception of sample PLB-93. Furthermore, some large chlorites oriented along S_1 are zoned, showing high-temperature relic cores (350-450 °C; see white insets in Fig. 4c-d) surrounded by low-temperature rims (150-250 °C).

To test Vidal et al. (2005, 2006) and Bourdelle et al. (2013) thermometers, an area of representative chlorites in an S_1 microlithon was selected from each map (see red insets in Fig. 4d). Corresponding chlorite compositions were extracted and introduced in the chlorite-quartz-water equilibria (Fig. 7a, Vidal et al., 2005, 2006; Fig. 7b, Bourdelle et al., 2013). The

temperature estimates (Fig. 7) derived from both methods are fairly similar, averaging 120-230 °C in sample PLB-88 and 150-380 °C in sample PLB-84. These estimates are also in agreement with the estimates derived from temperature maps calculated with the Lanari et al. (2014a) model. Only sample PLB-93 shows a divergence on temperature averages: mostly 150-250 °C with the thermometer of Bourdelle et al. (2013), and 250-350 °C with that of Vidal et al. (2005, 2006). In both cases (Bourdelle et al. (2013) and Vidal et al. (2005, 2006) methods), the higher temperature analyses are obtained from crystal cores in sample PLB-93.

4.3. RSCM thermometry

The ratio parameters and corresponding maximum temperatures obtained from all the spectra analyzed are shown in the supplementary information. The Raman spectra were decomposed into bands following the appropriate fitting procedure described in Beyssac et al. (2002a) for the lower formations (high-temperature Raman spectra; ratio parameter R2) and Lahfid et al. (2010) for the Santa Iría Formation (low-temperature Raman spectra; ratio parameters RA1 and RA2; Fig. 3). The average temperatures are shown in Table 1 and Fig. 1c with a relative colour bar from red (higher temperature) to blue (lower temperature). The average temperatures for the lower formations range from 420 to 530 °C, with a mean value of 468 °C (standard deviation of 35). The highest temperatures are found in samples PLB-82 (530 °C) and PLB-93 (495 °C), and estimates of the remaining samples do not exceed 480 °C. As for the Santa Iría Formation, temperatures are lower (315-330 °C; Table 1) than in the underlying formations.

5. Interpretation and discussion

5.1. Deformation/metamorphism relationships

The obtained analytical results are interpreted below in the context of the Variscan evolution of the Pulo do Lobo domain. As described above, two regional deformational events D₁ and D₂ yielded two foliations (Devonian S₁ and Carboniferous S₂) accompanied by metamorphic phyllosilicate growth (M₁ and M₂). In the cross-sections of Fig. 1c, KI values derived from XRD and average temperature from RSCM suggest that the lowest metamorphic grade (green and blue colours) corresponds to the Santa Iría Formation.

Textural observations suggest that in most samples of the lower formations M₁ was the main crystallization event, developing abundant and large-sized white mica and chlorite in S₁ microlithons, while M₂ generated small-sized white mica (e.g., Fig. 2e and map 1 in Fig. 4). On the other hand, polydeformed rocks commonly show previously grown minerals rotated towards a new foliation developed at lower-grade conditions, without new crystallization. This can be the case of the white micas that define S₂ in some samples (illustrated in Fig. 2d), which, in turn, is compatible with the similar chemical composition of S₁ and S₂ micas (Fig. 5a). As shown in these samples, S₁ is variably crenulated by D₂, implying M₁ minerals are variably rotated towards S₂. Consequently, the metamorphic data obtained from the samples of the lower formations will be ascribed to D₁-M₁. Sample PLB-93 might represent an exception, since its slightly higher RSCM and chlorite-derived temperatures could be due to

nearby intrusions (Fig. 1b and 1c.2; see below). In this respect, it is important to note the Mississippian transtensional event (basins development and abundant mafic magmatism) that took place between D₁ and D₂ (Pérez-Cáceres et al., 2015). The characterization of M₂ can be done by studying the samples from the Santa Iría Formation, which are only affected by S₂ accompanied by small-sized phyllosilicate growth (Fig. 2f). No crystallization has been observed related to the S₃ disjunctive crenulation cleavage.

5.2. First tectonothermal event (Devonian M₁)

The observed mineral assemblage (Qz + Ab + Ms + Chl ± Pg), together with the presence of C/S is compatible with low-grade metamorphic conditions (Table 1). White mica “crystallinity” values (0.17-0.22 $\Delta^{\circ}2\theta$; average 0.19) are consistently in the range of the epizone (low-grade or greenschists facies; >300 °C; Frey, 1987; Kisch, 1987, Warr and Ferreiro Mähnlmann, 2015), in accordance with the values reported by Abad et al. (2001) in a more general study of the diagenetic-metamorphic evolution of the South Portuguese Zone metapelites. Nevertheless, both the values of KI, far from 0.14 $\Delta^{\circ}2\theta$ (high epizone conditions according to Abad et al., 2006), and their variability, suggest that temperature was not high enough as to stabilize a highly crystalline white mica. This interpretation is in agreement with the low Na content of K-micas coexisting with paragonite (Fig. 6), implying a very-low temperature position in the muscovite-paragonite solvus for natural quasi-binary Pg-Ms pairs (Guidotti et al., 1994). By contrast, the maximum temperatures obtained from RSCM geothermometry are surprisingly high (420-530 °C; average 470 °C; corresponding to very high epizone or even medium-grade metamorphic conditions; Table 1).

The composition of paired chlorite and white mica is normally used to calculate pressure and temperature (e.g., Vidal et al., 2006), but the multi-equilibrium approach was not successful because the P-T equilibrium conditions did not converge. This result is indicative of chemical disequilibrium, precluding their use as a reliable geothermobarometer in this case. The temperatures calculated from chlorite compositions following various approaches (Vidal et al., 2006, Fig. 7a; Bourdelle et al., 2013, Fig. 7b; Lanari et al., 2014a, Fig. 4d) are as follow: 100-230 °C for sample PLB-88, 150-375 °C for sample PLB-84, and 150-450 °C for sample PLB-93 (Figs. d and 7, and Table 1). The slightly higher temperature of sample PLB-93 is inferred from its highest white mica “crystallinity” (0.17 $\Delta^{\circ}2\theta$), high RSCM temperature (495 °C), high-temperature (amesite-rich) chlorite and higher chlorite thermometry (Table 1), and can be explained by its proximity to metric-scale mafic igneous bodies of the Peramora Mélange (located at \approx 200 m to the south; Pérez-Cáceres et al., 2015) and/or to a granite stock (located at \approx 5 km to the west) (Fig. 1b).

In our samples there is some evidence of chlorite retrogression: (i) the chemical disequilibrium showed by the white mica/chlorite geothermobarometer, (ii) the presence of C/S mixed layers that are not stable in the epizone (e.g. Potel et al., 2006), (iii) the difference between temperature estimates from crystal rims to cores, and the higher temperature relic cores preserved in large chlorites defining S₁ (Fig. 4c-d), and (iv) the previously reported XRD and TEM data of chlorite retrograded to smectite and corrensite in the Pulo do Lobo domain (see fig. 1 in Nieto et al., 2005). The existence of chlorites with different compositions crystallized at different temperatures is the typical scenario (e.g., Vidal et al.,

2006, 2016; Lanari et al., 2012; 2014a and b; Grosch et al., 2012; 2014; Cantarero et al., 2014). In such situations, precise estimates of a single temperature and pressure attributable to peak conditions are really difficult to obtain. The maximum temperature showed by chlorite relic cores is 350-450 °C (Fig. 4d), which is consistent with the conditions estimated for M₁ by means of RSCM data.

An issue that deserves some discussion is the difference in temperature estimates between RSCM and other techniques. RSCM thermometry records the peak temperature and is not sensitive to the retrograde path. Alternatively, other methods based on phyllosilicate compositions are prone to record reequilibration during the retrograde path; thus, they rarely record the peak conditions, except perhaps in the core of certain large crystals. Therefore, RSCM and phyllosilicate-based methods do not record the same information on temperature, but are in fact complementary. The analyzed CM grains were carefully checked by microtextural observations and spectral geometry to ensure that these grains were actually derived from in situ organic matter graphitized during metamorphism.

In our case study, at the high peak temperature given by the RSCM thermometry, minerals such as biotite or garnet are expected to crystallize in metasedimentary rocks, though they have not been observed in our samples. Biotite has been said to exist in a few previous works (Apalategui et al., 1983; Braid et al., 2010; Rubio Pascual et al., 2013). However, in a few of our samples, biotite-looking crystals have resulted to be oxichlorites under SEM analyses. The absence or exceptional presence of biotite can be due to whole-rock composition, and explained by growth inhibition related to Na-excess, as evidenced by the presence of albite and paragonite in our samples. Another possible explanation could be the higher sensitivity of CM graphitization to rapid reequilibration during a short duration thermal event. Thus, the Mississippian intrusions subsequent to M₁ in the Pulo do Lobo Formation (see description in section 2) could have exerted a fast and locally intense thermal imprint that influenced CM but not the crystal chemistry of silicates. Moreover, recrystallization processes are not only a function of temperature, but are also promoted by deformation/stress, time, fluid/rock ratio (Merriman and Frey, 1999). Observations of this kind (differing reaction kinetics between organic and inorganic material (e.g. illite) in a contact metamorphic setting can be found in Olsson (1999) and Abad et al. (2014). Regarding the timing of geological processes, Mori et al. (2017) investigated the importance of heating duration for RSCM thermometry by studying graphitization around dykes. They showed that small-scale intrusions generating short thermal events modify the structure of CM in the surrounding rocks, and concluded that CM crystallinity is clearly related to contact metamorphism. The influence of low-pressure contact aureoles on RSCM temperature patterns is further supported by the results obtained by Hilchie and Jamieson (2014), who concluded that the variation of RSCM temperatures can be controlled by the subsurface geometry of a pluton. Finally, the long-distance thermal influence of plutonic intrusions on low-grade rocks located as far as 10 km has already been documented (e.g., Merriman and Frey, 1999; Martínez Poyatos et al., 2001) and could also be recorded by RSCM thermometry in our samples.

5.3. Second tectonothermal event (middle/upper Carboniferous M₂)

The mineralogy of the Santa Iría samples ($Qz + Fsp + Ms + Chl \pm C/S$) is compatible with very low- to low-grade conditions. The K-white mica “crystallinity” values (0.20-0.26 $\Delta^{\circ}2\theta$; average 0.23) point to lower epizone conditions, very close to the boundary with the anchizone ($\approx 300^{\circ}C$; Frey, 1987; Kisch, 1987). The temperatures calculated by RSCM in two samples (315 and $330^{\circ}C$) are compatible with the KI data of XRD analysis.

Our metamorphic data corroborate the existence of an unconformity between the lower and upper formations of the Pulo do Lobo domain (Pérez-Cáceres et al., 2015). Table 2 summarizes the relationship between deformation and metamorphism of the Pulo do Lobo domain in the context of the Variscan tectonic evolution of SW Iberia (Pérez-Cáceres et al., 2015). The lower formations record a Devonian tectonothermal event that reached epizone or lower greenschist facies conditions (M_1 with generalized phyllosilicate growth at temperatures as high as $450^{\circ}C$), whereas the overlying upper formation records a middle/upper Carboniferous tectonothermal event close to the anchizone/epizone boundary (M_2 with small-sized phyllosilicate growth at temperatures ≈ 300 - $330^{\circ}C$; Table 1). Obviously, M_2 also affected somehow the lower formations, being, at least in part, the responsible for the observed retrogression of M_1 chlorite and/or crystallization of new chlorites at lower temperature.

5.4. Pressure conditions

The measured b -cell parameters of K-white mica (in a short range between 8.991-9.002 Å; average 8.996; standard deviation 0.003) are very similar in the lower and upper formations of the Pulo do Lobo domain. Thus, the b parameter shows little variation and reflects very low phengite substitution in mica, as expected at low-pressure settings (Potel et al., 2006, 2016), near the intermediate pressure gradient boundary (Guidotti and Sassi, 1986).

In agreement with the low b -cell parameters, the composition of K-white mica is close to muscovite with very low celadonite and higher pyrophyllite content (Fig. 5a), as expected for illite-rich mica formed at low-pressure gradients. In the case of high- or medium-pressure conditions, a continuous trend in mica compositions would reflect the decompression path after the peak pressure, while the b -cell parameter would represent an average value of the range of mica compositions found in the sample (Abad et al., 2003b). On the contrary, at low-pressure settings, the overall range of recorded pressure is very restricted and micas present similar compositions and b -cell parameters among the various samples, as in the case of the Pulo do Lobo samples (Figs. 5a and 6, and Table 1).

The Pulo do Lobo domain has been classically interpreted as a pre-collisional subduction-related accretionary prism, based on the MORB geochemistry of their mafic rocks (see section 2.1). According to this classical interpretation, features typical of modern subduction systems should be expected, such as high-pressure metamorphic gradient remnants of partial subduction/exhumation in an accretionary wedge (e.g., Platt, 1986; Ernst, 2005), or slices of oceanic slab-derived lithologies (varied mid-ocean ridge metaigneous lithologies and also deep ocean bottom metasediments). Thus, recent works on the Makran accretionary prism (Omrani et al., 2017) and the subduction system of Japan (Endo and Wallis, 2017) describe an accretionary mélange complex composed of pelagic sedimentary rocks, ophiolites,

greenschists, amphibolites, and blueschists with high-pressure minerals such as lawsonite and glaucophane. However, most of the geological data concerning the Pulo do Lobo domain do not support such an interpretation (see section 2.1), and our new estimates of pressure conditions are also in disagreement. The only evidence supporting high-pressure gradient in the Pulo do Lobo domain is the interpretation of some rhomboidal aggregates of epidote porphyroblasts as the remnants of supposed lawsonite grown prior to S_2 in some samples in the Pulo do Lobo mafic schists (Rubio Pascual et al., 2013). However, no analytical data have been presented to support the presence of lawsonite pseudomorphs.

6. Conclusions

Eighteen samples of metapelites from the Pulo do Lobo domain have been studied to determine their Variscan low-grade metamorphic conditions. The microstructural analysis of the samples of the lower formations (Devonian Pulo do Lobo and Ribeira de Limas) shows the existence of two superposed low-grade tectonothermal events with associated foliation and phyllosilicate growth (S_1 - M_1 and S_2 - M_2 ; Table 2). M_2 was less intense, and is the only event that affected the overlying Carboniferous Santa Iria Formation. The regional geology also shows that a Mississippian thermal (magmatic) event occurred in-between M_1 and M_2 .

M_1 and M_2 correspond to chlorite zone metamorphism, but M_1 attained epizone conditions (greenschists facies with temperatures up to ≈ 450 °C), while M_2 did not exceed the anchizone-epizone boundary (≈ 300 °C).

The temperature estimates obtained from RSCM are higher than the estimates obtained from chlorite geothermometry and white mica data. This discrepancy can be explained by the fact that RSCM records the maximum temperature because of it is not affected by retrogression, in contrast with the other methods. In addition, this difference can be the consequence of the high sensitivity of CM to quickly re-equilibrate to maximum temperatures during short-duration thermal events such as the magmatic intrusions emplaced during the Mississippian thermal event.

Thermodynamic disequilibrium between white mica and chlorite has precluded their use for geothermobarometry, and a variety of data (including the existence of relic high-temperature chlorite cores, the presence of chlorite/smectite mixed layers, or the very-low temperatures calculated with chlorite geothermometers) indicate chlorite retrogression after M_1 metamorphic climax and crystallization of new chlorite grains at lower temperature.

The low-pressure conditions derived from white mica indicators (very low celadonite content and *b*-cell values) are incompatible with the high-pressure metamorphic gradient expected in a subduction-related accretionary wedge, which has been the classical interpretation of the Pulo do Lobo domain. Instead we interpret that the Pulo do Lobo rocks were deposited in a platform setting located near the northern border of Avalonia, but they were never involved in the subduction-related processes of the SPZ/OMZ suture.

Acknowledgements

This work was supported by the projects CGL2011-24101 (Spanish Ministry of Science and Innovation), CGL2015-71692-P and CGL2016-75679-P (Spanish Ministry of Economy and Competitiveness), RNM-148 and RNM-179 (Andalusian Government) and BES-2012-055754 (Doctoral scholarship to I. Pérez-Cáceres from the Spanish Ministry of Science and Innovation). The Raman facility in Paris has been funded by the City of Paris (Emergence program). We thank Valérie Magnin for her assistance with the microprobe analysis in Grenoble and Pierre Lanari for his support with thermodynamic software. Detailed revisions by C. Quesada, J.B. Murphy and an anonymous reviewer contributed to improve this paper.

Figure captions

Figure 1. a) Location of the studied area in the SW of the Iberian Massif (in grey). CIZ: Central Iberian Zone, OMZ: Ossa-Morena Zone, SPZ: South Portuguese Zone. b) Geological map of the Pulo do Lobo domain and other units related to the OMZ/SPZ boundary with indications of the two cross-sections studied and collected samples. c.1-2) Geological cross-sections of the Pulo do Lobo domain (see b for location) (modified from Martínez Poza et al., 2012 and Pérez-Cáceres et al., 2015). Numbered red circles in b-c locate the samples studied. Big circles show the KI values for 10 Å reflection peaks of K-white mica and the average RSCM temperatures, with the relative colour bar according to the results shown in Table 1. BAA: Beja-Acebuches Amphibolites, M: metabasalts, PL: Pulo do Lobo Formation, RL: Ribeira de Limas Formation, SI: Santa Iría Formation.

Figure 2. Pictures of the Pulo do Lobo rocks illustrating deformation at outcrop scale: a) Pulo do Lobo formation, b) Ribeira de Limas Formation, c) Santa Iría Formation. Microphotographs from thin-sections: d) Cross-polarized light image of sample PLB-84 (Pulo do Lobo Formation), e) SEM-BSE image of sample PLB-88 (Ribeira de Limas Formation), f) Cross-polarized light images of sample PLB-71 (Santa Iría Formation).

Figure 3. Representative Raman spectra of CM across the Pulo do Lobo domain from low temperature (bottom; Santa Iría Formation) to high temperature (top; lower formations) including the average maximum temperatures (°C) for each sample. Vertical scale for spectrum intensity is arbitrary. See Fig. 1 for sample location and Table 1 and supplementary information for RSCM data.

Figure 4. X-Ray maps of the three selected samples analyzed by EPMA and processed with XMapTools. The samples belong to the lower formations of the Pulo do Lobo domain (sample PLB-88: Ribeira de Limas Formation; samples PLB-84 and PLB-93: Pulo do Lobo Formation; the latter (PLB-93) is close to Early Carboniferous igneous intrusions). a) EPMA BSE photographs. b) Mineral maps. c) Al^{IV} content map in chlorites, which increases with temperature. The white square highlights the zonation of a chlorite grain from core to rim. d) Temperature maps of chlorite using the Lanari et al. (2014a) geothermometer assuming all iron as ferrous. White squares show selected areas illustrating higher-temperature chlorite cores. Red squares show the selected areas (representative of S₁ foliation) used for chlorite-quartz-water geothermometric calculations shown in Fig. 7.

Figure 5. Ternary plots of all the analyzed white micas (a) (Cel: celadonite, Mus: muscovite, Prl: pyrophyllite) and chlorite (b) (Cli+Daph: clinochlore + daphnite, Am: amesite, Sud: sudoite) plotted with the XmapTools TriPlot3D module. Colour bars refer to the number of mica/chlorite pixels analyzed.

Figure 6. Compositional diagram of white micas showing Na/(Na+K) vs Si/Al (atomic ratios) for 31 EPMA point analyses from seven samples of the lower formations of the Pulo do Lobo domain

(different symbology, for each sample). Point analyses were obtained on the microprobe at the University of Huelva (Spain). Qualitative information about temperature and pressure conditions are respectively according to Guidotti et al. (1994), Coggon and Holland (2002), Parra et al. (2002), Massonne and Schreyer (1987) and Massonne and Szpurka (1997).

Figure 7. Histograms of temperatures obtained using the chlorite-quartz-water geothermometer of Vidal et al. (2006) (a) and Bourdelle et al. (2013) (b) on selected representative S₁ chlorites (see red squares in Fig. 4d for location). *n* represents the number of chlorites that could be used for each calibration. The number of analyses is lower in those with Vidal et al. (2006) approach because the assumption that the Si content of chlorite is lower than 3 apfu.

Table captions

Table 1. Samples and results obtained by XRD (<2 µm fraction), white mica and chlorite compositions, temperature ranges from chlorite thermometry, and average RSCM thermometry. Basel KI values and average RSCM temperatures show a relative colour-bar scale. Mineral abbreviations according to Whitney & Evans (2010). Qz: Quartz, Ms: Muscovite, Fsp: Feldspar, Chl: Chlorite, Pg: paragonite, C/S: chlorite-smectite mixed layers, Cel: celadonite, Prl: pyrophyllite, Cli+Daph: clinochlore + daphnite, Am: amesite, Sud: sudoite, Std Dv: standard deviation.

Table 2. Summary of the tectonometamorphic Variscan evolution of the Pulo do Lobo domain.

References

- Abad, I., Mata, M.P., Nieto, F., and Velilla, N.: The phyllosilicates in diagenetic-metamorphic rocks of the South Portuguese Zone, southwestern Portugal, *The Canadian Mineralogist*, 39(6), 1571-1589, 2001.
- Abad, I., Nieto, F., and Velilla, N.: Chemical and textural characterisation of diagenetic to low-grade metamorphic phyllosilicates in turbidite sandstones of the South Portuguese Zone: A comparison between metapelites and sandstones, *Schweizerische Mineralogische und Petrographische Mitteilungen*, 82(2), 303-324. 2002.
- Abad, I., Nieto, F., and Gutiérrez-Alonso, G.: Textural and chemical changes in slate-forming phyllosilicates across the external-internal zones transition in the low-grade metamorphic belt of the NW Iberian Variscan Chain, *Swiss Bulletin of Mineralogy and Petrology*, 83(1), 63-80, 2003a.
- Abad, I., Gutierrez-Alonso, G., Nieto, F., Gertner, I., Becker, A., and Cabero, A.: The structure and the phyllosilicates (chemistry, crystallinity and texture) of Talas Ala-Tau (Tien Shan, Kyrgyz Republic); comparison with more recent subduction complexes, *Tectonophysics*, 365(1-4), 103-127, 2003b.
- Abad, I., Nieto, F., Gutiérrez-Alonso, G., Campo, M. D., López-Munguira, A., and Velilla, N.: Illitic substitution in micas of very low-grade metamorphic clastic rocks. *European Journal of Mineralogy*, 18(1), 59-69, 2006.
- Abad, I., Nieto, F., Velilla, N., and Suárez-Ruiz, I.: Metamorphic evidences from the Monchique pluton (South Portugal): Contact metamorphism vs regional metamorphism under very low-grade conditions, *Revista de la Sociedad Geológica de España*, 27(1): 337-350, 2014.

- 743 Abalos, B., Gil Ibarguchi, J.I., and Eguluz, L.: Cadomian subduction/collision and Variscan
744 transpression in the Badajoz-Córdoba shear belt, southwest Spain, *Tectonophysics*, 199, 51-
745 72, 1991.
- 746 Airaghi, L., Lanari, P., de Sigoyer, J., and Guillot, S.: Microstructural vs compositional preservation
747 and pseudomorphic replacement of muscovite in deformed metapelites from the Longmen
748 Shan (Sichuan, China), *Lithos*, 282, 262-280, 2017.
- 749 Ali, A.: The tectono-metamorphic evolution of the Balcooma Metamorphic Group, north-eastern
750 Australia: a multidisciplinary approach, *Journal of Metamorphic Geology*, 28(4), 397-422,
751 2010.
- 752 Apalategui, O., Barranco, E., Contreras, F., Delgado, M., and Roldán, F. J.: Hoja 916, Aroche, Mapa
753 Geológico de España a escala 1:50000, Inst. Geológico y Minero de España, Madrid, 1983.
- 754 Araújo, A., Fonseca, P., Munhá, J., Moita, P., Pedro, J., and Ribeiro, A.: The Moura Phyllonitic
755 Complex: an accretionary complex related with obduction in the southern Iberia Variscan
756 suture, *Geodinamica Acta*, 18, 375-388, 2005.
- 757 Arenas, R., Abati, J., Martínez Catalán, J.R., García, F. D., and Pascual, F.R.: PT evolution of eclogites
758 from the Agualada Unit (Ordenes Complex, northwest Iberian Massif, Spain): Implications
759 for crustal subduction, *Lithos*, 40(2), 221-242, 1997.
- 760 Azor, A., González Lodeiro, F., and Simancas, J.F.: Tectonic evolution of the boundary between the
761 Central Iberian and Ossa-Morena zones (Variscan Belt, southwest Spain), *Tectonics*, 13, 45-
762 61, 1994.
- 763 Azor, A., Rubatto, D., Simancas, J.F., González Lodeiro, F., Martínez Poyatos, D., Martín Parra L.M.,
764 and Matas, J.: Rheic Ocean ophiolitic remnants in Southern Iberia questioned by SHRIMP
765 U-Pb zircon ages on the Beja-Acebuches amphibolites, *Tectonics*, 27(5), 2008.
- 766 Azor, A., Simancas, J.F., Martínez Poyatos, D., Pérez-Cáceres, I., González Lodeiro, F., and Expósito,
767 I.: Chapter 10.3: Deformation and Structure, Southwestern Iberia, in: *The Geology of Iberia:
768 A Geodynamic Approach*, Volume 2: The Variscan Cycle, edited by: Quesada, C., and
769 Oliveira, J.T., Springer, 316-335, 2019.
- 770 Barbero, L.: Granulite-facies metamorphism in the Anatectic Complex of Toledo, Spain: late
771 Hercynian tectonic evolution by crustal extension, *Journal of the Geological Society*, 152(2),
772 365-382, 1995.
- 773 Bard, J.P. : Signification tectonique des métatholeites d'anité abyssale de la ceinture de base pression
774 d'Aracena (Huelva, Espagne), *Bulletin de la Société Géologique de France*, 19, 385-393,
775 1977.
- 776 Bastida, F., Martínez-Catalán, J.R., and Pulgar, J.A.: Structural, metamorphic and magmatic history
777 of the Mondoñedo nappe (Hercynian belt, NW Spain). *Journal of Structural Geology*, 8(3-
778 4), 415-430, 1986.
- 779 Bastida, F., Brime, C., García-López, S. Aller, J., Valín, M.L., and Sanz-López, J.: Tectono-thermal
780 evolution of the Cantabrian Zone (NW Spain), in: *Palaeozoic conodonts from northern
781 Spain*, edited by: García López, S., and Bastida, F., Instituto Geológico y Minero de España,
782 Cuadernos del Museo Geominero, 1, 105-123, Madrid, ISBN: 84-7840-446-5, 2002.
- 783 Battaglia, S., Leoni, L., and Sartori, F.: The Kübler index in late diagenetic to low-grade metamorphic
784 pelites: a critical comparison of data from 10 Å and 5 Å peaks, *Clays and Clay Minerals*,
785 52(1), 85-105, 2004.

786 Beyssac, O., Goffé, B., Chopin, C., and Rouzaud, J.N.: Raman spectra of carbonaceous material in
787 metasediments: a new geothermometer, *Journal of Metamorphic Geology*, 20, 859-871,
788 2002a.

789 Beyssac, O., Rouzaud, J.-N., Goffé, B., Brunet, F., and Chopin, C.: Graphitization in a high-pressure,
790 low temperature metamorphic gradient: a Raman microspectroscopy and HRTEM study.
791 *Contrib. Mineral. Petrol.*, 143, 19-31, 2002b.

792 Beyssac, O., Goffé, B., Petitet, J.P., Froigneux, E., and Rouzaud, J.N.: On the characterization of
793 disordered and heterogeneous carbonaceous materials using Raman spectroscopy,
794 *Spectrochim. Acta A Mol. Biomol. Spectrosc.*, 59, 2267-2276, 2003.

795 Beyssac, O., Bollinger, L., Avouac, J.P., and Goffé, B.: Thermal metamorphism in the lesser Himalaya
796 of Nepal determined from Raman spectroscopy of carbonaceous material, *Earth and*
797 *Planetary Science Letters*, 225, 233-241, 2004.

798 Booth-Rea, G., Simancas, J.F., Azor, A., Azañón, J.M., Gonzalez Lodeiro, F., and Fonseca, P.: HP-
799 LT Variscan metamorphism in the Cubito-Moura schists (Ossa-Morena Zone, southern
800 Iberia), *Comptes Rendus Geoscience*, 338(16), 1260-1267, 2006.

801 Bourdelle, F., Parra, T., Chopin, C., and Beyssac, O.: A new chlorite geothermometer for diagenetic
802 to low-grade metamorphic conditions, *Contributions to Mineralogy and Petrology*, 165(4),
803 723-735, 2013.

804 Bousquet, R., Oberha, R., Goffé, B., Wiederkehr, M., Koller, F., Schmid, S.M., Schuster, R., Engi,
805 M., Berger, A., and Martinotti, G.: Metamorphism of metasediments at the scale of an
806 orogen: a key to the tertiary geodynamic evolution of the Alps, *Geological Society, London,*
807 *Special Publications*, 298, 393-411, 2008.

808 Braid, J.A., Murphy, J.B., and Quesada, C.: Structural analysis of an accretionary prism in a continental
809 collisional setting, the Late Paleozoic Pulo do Lobo Zone, Southern Iberia, *Gondwana*
810 *Research*, 17(2-3), 422-439, 2010.

811 Braid, J. A., Murphy, J. B., Quesada, C., and Mortensen, J.: Tectonic escape of a crustal fragment
812 during the closure of the Rheic Ocean: U–Pb detrital zircon data from the Late Palaeozoic
813 Pulo do Lobo and South Portuguese zones, southern Iberia, *Journal of the Geological*
814 *Society*, 168(2), 383-392, 2011.

815 Braid, J. A., Murphy, J. B., Quesada, C., Gladney, E. R. and Dupuis, N.: Progressive magmatism and
816 evolution of the Variscan suture in southern Iberia. *International Journal of Earth Sciences*,
817 107(3), 971-983, 2018.

818 Brown, M.: P–T–t evolution of orogenic belts and the causes of regional metamorphism, *Journal of*
819 *the Geological Society*, 150(2), 227-241, 1993.

820 Burg, J.P., Iglesias, M., Laurent, P., Matte, P., and Ribeiro, A.: Variscan intracontinental deformation:
821 the Coimbra-Córdoba Shear zone (SW Iberian Peninsula), *Tectonophysics*, 78, 161-177,
822 1981.

823 Cantarero, I., Lanari, P., Vidal, O., Alías, G., Travé, A., and Baqués, V.: Long-term fluid circulation
824 in extensional faults in the central Catalan Coastal Ranges: P–T constraints from neoformed
825 chlorite and K-white mica, *International Journal of Earth Sciences*, 103(1), 165-188, 2014.

826 Castro, A., Fernández, C., De la Rosa, J.D., Moreno Ventas, I., and Rogers, G.: Significance of
827 MORB-derived amphibolites from the Aracena metamorphic belt, southwest Spain, *Journal*
828 *of Petrology*, 37(2), 235-260, 1996.

- 829 Castro, A., Fernández, C., El-Hmidi, H., El-Biad, M., Díaz, M., De la Rosa, J., and Stuart, F.: Age
830 constraints to the relationships between magmatism, metamorphism and tectonism in the
831 Aracena metamorphic belt, southern Spain, *International Journal of Earth Sciences*, 88(1),
832 26-37, 1999.
- 833 Cathelineau, M.: Cation site occupancy in chlorites and illites as a function of temperature, *Clay*
834 *Minerals* 23, 471-485, 1988.
- 835 Cathelineau, M., and Nieva, D.: A chlorite solid solution geothermometer the Los Azufres (Mexico)
836 geothermal system, *Contrib. Mineral Petrol.*, 91(3), 235-244, 1985.
- 837 Coggon, R., and Holland, T.J.B.: Mixing properties of phengitic micas and revised garnet-phengite
838 thermobarometers, *Journal of Metamorphic Geology*, 20(7), 683-696, 2002.
- 839 Crespo-Blanc, A. and Orozco, M.: The Southern Iberian Shear Zone: a major boundary in the
840 Hercynian folded belt. *Tectonophysics*, 148(3-4), 221-227, 1988.
- 841 Crespo-Blanc, A.: Evolución geotectónica del contacto entre la zona de Ossa-Morena y la zona
842 Surportuguesa en las sierras de Aracena y Aroche (Macizo Ibérico Meridional): Un contacto
843 mayor en la cadena Hercínica Europea, Ph.D. Thesis, Univ. de Granada, 327 pp., 1991.
- 844 Crouzet, C., Dunkl, I., Paudel, L., Arkai, P., Rainer, T.M., Balogh, K., and Appel, E.: Temperature
845 and age constraints on the metamorphism of the Tethyan Himalaya in Central Nepal: A
846 multidisciplinary approach, *Journal of Asian Earth Sciences*, 30(1), 113-130, 2007.
- 847 Dahn, D.R.L., Braid, J.A., Murphy, J.B., Quesada, C., Dupuis, N., and McFarlane C.R.M.:
848 Geochemistry of the Peramora Melange and Pulo do Lobo schist: Geochemical investigation
849 and tectonic interpretation of mafic melange in the Pangean suture zone, Southern Iberia,
850 *International Journal of Earth Sciences*, 103(5), 1415-1431, 2014.
- 851 Dallmeyer, R.D., Fonseca, P.E., Quesada, C., and Ribeiro, A.: $^{40}\text{Ar}/^{39}\text{Ar}$ mineral age constraints for
852 the tectonothermal evolution of a variscan suture in Southwest Iberia, *Tectonophysics*, 222,
853 177-194, 1993.
- 854 De Andrade, V., Vidal, O., Lewin, E., O'Brien, P., and Agard, P.: Quantification of electron
855 microprobe compositional maps of rock thin sections: an optimized method and examples,
856 *Journal of Metamorphic Geology*, 24(7), 655-668, 2006.
- 857 Díaz Azpiroz, M., Fernández, C., Castro, A., and El-Biad, M.: Tectonometamorphic evolution of the
858 Aracena metamorphic belt (SW Spain) resulting from ridge-trench interaction during
859 Variscan plate convergence, *Tectonics*, 25(1), 2006.
- 860 Eden, C.P.: Tectonostratigraphic analysis of the northern extent of the oceanic exotic terrane,
861 Northwestern Huelva Province, Spain, Ph. D. Thesis, Univ. of Southampton, 214 pp., 1991.
- 862 Eden, C., and Andrews, J.: Middle to upper Devonian melanges in SW Spain and their relationship
863 to the Meneage formation in south Cornwall. *Proc. Ussher Soc.*, 7, 217-222, 1990.
- 864 Endo, S., and Wallis, S.R.: Structural architecture and low-grade metamorphism of the Mikabu-
865 Northern Chichibu accretionary wedge, SW Japan, *Journal of Metamorphic Geology*, 35(6),
866 695-716, 2017.
- 867 Ernst, W.G.: Tectonic history of subduction zones inferred from retrograde blueschist PT paths,
868 *Geology* 16(12), 1081-1084, 1988.
- 869 Ernst, W.G.: Alpine and Pacific styles of Phanerozoic mountain building: subduction-zone
870 petrogenesis of continental crust, *Terra Nova*, 17(2), 165-188, 2005.

871 Escuder Viruete, J., Arenas, R., and Martínez Catalán, J.R.: Tectonothermal evolution associated with
872 Variscan crustal extension in the Tormes gneiss dome (NW Salamanca, Iberian Massif,
873 Spain), *Tectonophysics*, 238(1-4), 117-138, 1994.

874 Fonseca, P., and Ribeiro, A.: Tectonics of the Beja-Acebuches ophiolite - a major suture in the Iberian
875 variscan foldbelt, *Geol. Rundsch.*, 82, 440-447, 1993.

876 Fonseca, P., Munhá, J., Pedro, J., Rosas, F., Moita, P., Araujo, A., and Leal, N.: Variscan ophiolites
877 and high-pressure metamorphism in southern Iberia. *Ophioliti*, 24, 259-268, 1999.

878 Franceschelli, M., Leoni, L., Memmi, I., and Puxeddu, M.: Regional distribution of Al-silicates and
879 metamorphic zonation in the low-grade Verrucano metasediments from the Northern
880 Apennines, Italy, *Journal of Metamorphic Geology*, 4(3), 309-321, 1986.

881 Frey, M.: Very low-grade metamorphism of clastic sedimentary rocks, in: *Low temperature*
882 *metamorphism*, edited by: Frey, M., Blackie, Glasgow, 9-58, 1987.

883 Frey, M., and Robinson, D.: *Low-Grade Metamorphism*, 313 pp. Blackwell Science Ltd, Cambridge,
884 1999.

885 Gil Ibarguchi, J., Mendiá, M., Girardeau, J., and Peucat, J.J.: Petrology of eclogites and clinopyroxene-
886 garnet metabasites from the Cabo Ortegal Complex (northwestern Spain), *Lithos*, 25(1-3),
887 133-162, 1990.

888 Goffé, B., and Velde, B.: Contrasted metamorphic evolutions in thrust cover units of the
889 Briançonnais zone (French Alps): A model for the conservation of HP-LT metamorphic
890 mineral assemblages, *Earth and Planetary Science Letters*, 68(2), 351-360, 1984.

891 Grosch, E.G., Vidal, O., Abu-Alam, T., and McLoughlin, N.: P-T constraints on the metamorphic
892 evolution of the Paleoproterozoic Kromberg type-section, Barberton greenstone belt, South
893 Africa, *Journal of Petrology*, 53(3), 513-545, 2012.

894 Grosch, E.G., McLoughlin, N., Lanari, P., Erambert, M., and Vidal, O.: Microscale mapping of
895 alteration conditions and potential biosignatures in basaltic-ultramafic rocks on early Earth
896 and beyond, *Astrobiology*, 14(3), 216-228, 2014.

897 Guidotti, C.V., and Sassi, F.P.: Classification and correlation of metamorphic facies series by means
898 of muscovite b data from low-grade metapelites, *Neues Jahrbuch für Mineralogie-*
899 *Abhandlungen*, 153, 363-380, 1986.

900 Guidotti, C. V., Mazzoli, C., Sassi, F. P., and Blencoe, J. G.: Compositional controls on the cell
901 dimensions of 2M 1 muscovite and paragonite, *European Journal of Mineralogy*, 4(2), 283-
902 297, 1992.

903 Guidotti, C.V., Sassi, F.P., Blencoe, J.G., and Selverstone, J.: The paragonite–muscovite solvus: I. P-
904 T-X limits derived from the Na – K compositions of natural, quasibinary paragonite-
905 muscovite pairs, *Geoch. Cosmochim. Acta*, 58, 2269–2275, 1994.

906 Gutiérrez-Alonso, G., and Nieto, F.: White-mica 'crystallinity', finite strain and cleavage development
907 across a large Variscan structure, NW Spain, *Journal of the Geological Society*, 153(2), 287-
908 299, 1996.

909 Hilchie, L.J., and Jamieson, R.A.: Graphite thermometry in a low-pressure contact aureole, Halifax,
910 Nova Scotia, *Lithos*, 208, 21-33, 2014.

911 Jarosewich, E.J., Nelen, J.A., and Norberg, J.A.: Reference samples for electron microprobe analysis:
912 *Geostandards Newsletter*, 4, 43-47, 1980.

- 913 Kisch, H.J.: Correlation between indicators of very low-grade metamorphism. In: Low temperature
914 metamorphism, edited by: Frey, M., Blackie, Glasgow, 227-300, 1987.
- 915 Kisch, H.J.: Illite crystallinity: recommendations on sample preparation, X-ray diffraction settings,
916 and interlaboratory samples, *Journal of Metamorphic Geology*, 9, 665–670, 1991.
- 917 Kübler, B. : Evaluation quantitative du metamorphism par la cristallinite de l'Illite. *Bull. Centres Rech.*
918 *Pau-SNPA* 2, 385-397, 1968.
- 919 Lahfid, A., Beyssac, O., Deville, E., Negro, F., Chopin, C., and Goffé, B.: Evolution of the Raman
920 spectrum of carbonaceous material in low-grade metasediments of the Glarus Alps
921 (Switzerland), *Terra Nova*, 22, 354-360, 2010.
- 922 Lanari, P., Guillot, S., Schwartz, S., Vidal, O., Tricart, P., Riel, N., and Beyssac, O. : Diachronous
923 evolution of the alpine continental subduction wedge: evidence from P-T estimates in the
924 Briançonnais Zone houillère (France-Western Alps), *Journal of Geodynamics*, 56-57, 39-54,
925 2012.
- 926 Lanari, P., Vidal, O., de Andrade, V., Dubacq, B., Lewin, E., Grosch, E.G., and Schwartz, S.:
927 XMapTools: A MATLAB©-based program for electron microprobe X-Ray image
928 processing and geothermobarometry, *Computers & Geosciences*, 62, 227-240, 2014a.
- 929 Lanari, P., Rolland, Y., Schwartz, S., Vidal, O., Guillot, S., Tricart, P., and Dumont, T.: P–T–t
930 estimation of deformation in low-grade quartz-feldspar-bearing rocks using thermodynamic
931 modelling and $^{40}\text{Ar}/^{39}\text{Ar}$ dating techniques: example of the Plan-de-Phasy shear zone unit
932 (Briançonnais Zone, Western Alps), *Terra Nova*, 26(2), 130-138, 2014b.
- 933 Lopes, G., Pereira, Z., Fernandes, P., Wicander, R., Matos, J.X., Rosa, D., and Oliveira, J.T.: The
934 significance of reworked palynomorphs (middle Cambrian to Tournaisian) in the Viséan
935 Toca da Moura Complex (South Portugal). Implications for the geodynamic evolution of
936 Ossa Morena Zone, *Rev. Palaeobot. Palynol.*, 200, 1-23, 2014.
- 937 López-Carmona, A., Pitra, P., and Abati, J.: Blueschist-facies metapelites from the Malpica-Tui Unit
938 (NW Iberian Massif): phase equilibria modelling and H₂O and Fe₂O₃ influence in high-
939 pressure assemblages, *Journal of Metamorphic Geology*, 31(3), 263-280, 2013.
- 940 López Munguira, A., Nieto, F., Pardo, E. S., and Velilla, N.: The composition of phyllosilicates in
941 Precambrian, low-grade metamorphic, clastic rocks from the Southern Hesperian Massif
942 (Spain) used as an indicator to metamorphic conditions, *Precambrian Research*, 53(3-4), 267-
943 279, 1991.
- 944 López Sánchez-Vizcaíno, V., Gómez Pugnaire, M.T., Azor, A., and Fernández Soler, J.M.: Phase
945 diagram sections applied to amphibolites: a case study from the Ossa-Morena/Central
946 Iberian Variscan suture (Southwestern Iberian Massif), *Lithos*, 68, 1-21, 2003.
- 947 Martínez Catalán, J.R.: Estratigrafía y estructura del Domo de Lugo (Sector Oeste de la Zona
948 Asturoccidental-leonesa), *Corpus Geol. Gallaeacae* (2º Serie), 2, 1-291, 1985.
- 949 Martínez Catalán, J.R., Rubio Pascual, F.J., Díez Montes, A., Díez Fernández, R., Gómez Barreiro,
950 J., Dias Da Silva, Í., González Clavijo, E., Ayarza, P., and Alcock, J.E.: The late Variscan
951 HT/LP metamorphic event in NW and Central Iberia: relationships to crustal thickening,
952 extension, orocline development and crustal evolution, *Geological Society, London, Special*
953 *Publications*, 405(1), 225-247, 2014.
- 954 Martínez Poyatos, D., Nieto, F., Azor, A., and Simancas, J.F.: Relationships between very low-grade
955 metamorphism and tectonic deformation: Examples from the southern Central Iberian Zone
956 (Iberian Massif, Variscan Belt), *Journal of the Geological Society*, 158, 953-968, 2001.

- 957 Martínez Poza, A.I., Martínez Poyatos, D., Simancas, J.F., and Azor, A.: La estructura varisca de la
958 Unidad del Pulo do Lobo (SO del Macizo Ibérico) en las transversales de Aroche y Rosal de
959 la Frontera (Huelva), *Geogaceta*, 52, 21-24, 2012.
- 960 Massonne, H.J., and Schreyer, W.: Phengite geobarometry based on the limiting assemblage with K-
961 feldspar, phlogopite, and quartz, *Contributions to Mineralogy and Petrology*, 96, 212-224,
962 1987.
- 963 Massonne, H.J., and Szpurka, Z.: Thermodynamic properties of white micas on the basis of high-
964 pressure experiments in the systems K_2O - MgO - Al_2O_3 - SiO_2 - H_2O and K_2O - FeO - Al_2O_3 -
965 SiO_2 - H_2O . *Lithos*, 41, 229-250, 1997.
- 966 Matte, P.: The Variscan collage and orogeny (480-290 Ma) and the tectonic definition of the Armorica
967 microplate: A review, *Terra Nova*, 13, 122-128, 2001.
- 968 Merriman, R.J., and Frey, M.: Patterns of very low-grade metamorphism in metapelitic rocks, in: Low-
969 grade metamorphism, edited by: Frey, M., and Robinson, D., Blackwell, Oxford, 61-107,
970 1999.
- 971 Moita, P., Munhá, J., Fonseca, P., Pedro, J., Araújo, A., Tassinari, C., and Palacios, T.: Phase equilibria
972 and geochronology of Ossa-Morena eclogites, *Actas do XIV Semana de Gequímica / VIII*
973 *Congresso de geoquímica dos Países de Língua Portuguesa*, 2, 471-474, 2005.
- 974 Moore, D.M., and Reynolds, R.C. Jr.: X-ray Diffraction and the Identification and Analysis of Clay
975 Minerals, 2nd edition, Oxford University Press, Oxford, 1997.
- 976 Mori, H., Mori, N., Wallis, S., Westaway, R., and Annen, C.: The importance of heating duration for
977 Raman CM thermometry: evidence from contact metamorphism around the Great Whin Sill
978 intrusion, UK, *Journal of Metamorphic Geology*, 35(2), 165-180, 2017.
- 979 Munhá, J.: Metamorphic evolution of the south Portuguese/Pulo do Lobo zone, in: Pre-Mesozoic
980 Geology of Iberia, edited by: Dallmeyer, R.D., and Martínez García, E., Springer, Berlin,
981 Germany, pp. 363-368, 1990.
- 982 Munhá, J., Oliveira, J.T., Ribeiro, A., Oliveira, V., Quesada, C. and Kerrich, R.: Beja-Acebuches
983 ophiolite, characterization and geodynamic significance, *Maleo*, 2, 31, 1986.
- 984 Murphy, J. B., Quesada, C., Gutiérrez-Alonso, G., Johnston, S. T. and Weil, A.: Reconciling
985 competing models for the tectono-stratigraphic zonation of the Variscan orogen in Western
986 Europe. *Tectonophysics*, 681, 209-219, 2016.
- 987 Nieto, F., and Sánchez-Navas, A.: A comparative XRD and TEM study of the physical meaning of
988 the white mica «crystallinity» index, *European Journal of Mineralogy*, 6(5), 611-621, 1994.
- 989 Nieto, F., Mata, M.P., Bauluz, B., Giorgetti, G., Árkai, P., and Peacor, D.R.: Retrograde diagenesis, a
990 widespread process on a regional scale, *Clay Minerals*, 40(1), 93-104, 2005.
- 991 Oliveira, J.T.: Part VI: South Portuguese Zone, stratigraphy and synsedimentary tectonism, in: Pre-
992 Mesozoic Geology of Iberia, edited by: Dallmeyer, R.D., and Martínez García, E., Springer,
993 Berlin, Germany, pp. 334-347, 1990.
- 994 Olsson, I.: Regional burial heating vs. local magmatic heat influence of the Röstänga area, Scania,
995 southern Sweden, *GFF*, 121(3), 209-214, 1999.
- 996 Omrani, H., Moazzen, M., Oberhänsli, R., and Moslempour, M.E.: Iranshahr blueschist: subduction
997 of the inner Makran oceanic crust, *Journal of Metamorphic Geology*, 35(4), 373-392, 2017.

998 Ordóñez-Casado, B.: Geochronological studies of the Pre-Mesozoic basement of the Iberian Massif:
999 the Ossa-Morena Zone and the Allochthonous Complexes within the Central Iberian Zone,
1000 Ph.D. Thesis, ETH Zurich, 235 pp., 1998.

1001 Parra, T., Vidal, O., and Agard, P., A thermodynamic model for Fe-Mg dioctahedral K White micas
1002 using data from phase-equilibrium experiments and natural pelitic assemblages, *Contrib.*
1003 *Mineral Petrol.*, 143, 706-732, 2002.

1004 Pedro, J., Araujo, A., Fonseca, P., Tassinari, C., and Ribeiro, A.: Geochemistry and U-Pb Zircon Age
1005 of the Internal Ossa-Morena Zone Ophiolite Sequences: A Remnant of Rheic Ocean in SW
1006 Iberia, *Ophioliti*, 35(2), 117-130, 2010.

1007 Pereira, M.F., Apraiz, A., Chichorro, M., Silva, J.B., and Armstrong, R.A.: Exhumation of high
1008 pressure rocks in northern Gondwana during the Early Carboniferous (Coimbra-Cordoba
1009 shear zone, SW Iberian Massif): tectonothermal analysis and U-Th-Pb SHRIMP in-situ
1010 zircon geochronology, *Gondwana Research*, 17, 440-460, 2010.

1011 Pereira, M.F., Chichorro, M., Silva, J.B., Ordóñez-Casado, B., Lee, J.K., and Williams, I.S.: Early
1012 carboniferous wrenching, exhumation of high-grade metamorphic rocks and basin instability
1013 in SW Iberia: constraints derived from structural geology and U-Pb and ^{40}Ar - ^{39}Ar
1014 geochronology, *Tectonophysics*, 558, 28-44, 2012.

1015 Pereira, M.F., Chichorro, M., Williams, I.S., Silva, J.B., Fernández, C., Díaz-Azpíroz, M., Apraiz, A.,
1016 and Castro, A.: Variscan intra-orogenic extensional tectonics in the Ossa-Morena Zone
1017 (Évora-Aracena-Lora del Río metamorphic belt, SW Iberian Massif): SHRIMP zircon U-Th-
1018 Pb geochronology, *Geological Society, London, Special Publications*, 327(1), 215-237, 2009.

1019 Pereira, M.F., Martínez Poyatos, D., Pérez-Cáceres, I., Gama, C., and Azor, A.: Comment on
1020 “Stratigraphy of the Northern Pulo do Lobo Domain, SW Iberia Variscides: A palynological
1021 contribution” by Pereira, Z. et al. (2018) - *Geobios*, 51, 491-506. *Geobios*, in press, 2019.

1022 Pereira, Z., Matos, J., Fernandes, P., and Oliveira, J.T.: Palynostratigraphy and systematic palynology
1023 of the Devonian and Carboniferous successions of the South Portuguese Zone, Portugal,
1024 *Memórias Geológicas do Instituto Nacional de Engenharia, Tecnologia e Inovação* 34,
1025 Lisboa, 2008.

1026 Pereira, Z., Fernandes, P., Matos, J., Jorge, R., and Oliveira, J.T.: Stratigraphy of the Northern Pulo
1027 do Lobo Domain, SW Iberia Variscides: A palynological contribution, *Geobios*, 51, 491-506,
1028 2018.

1029 Pérez-Cáceres, I., Martínez Poyatos, D., Simancas, J.F., and Azor, A.: The elusive nature of the Rheic
1030 Ocean in SW Iberia, *Tectonics*, 34, 2429-2450, 2015.

1031 Pérez-Cáceres, I., Simancas, J.F., Martínez Poyatos, D., and Azor, A.: Oblique collision and
1032 deformation partitioning in the SW Iberian Variscides, *Solid Earth*, 7, 857-872, 2016.

1033 Pérez-Cáceres, I., Martínez Poyatos, D., Simancas, J.F., and Azor, A.: Testing the Avalonian affinity
1034 of the South Portuguese Zone and the Neoproterozoic evolution of SW Iberia through
1035 detrital zircon populations, *Gondwana Research*, 42, 177-192, 2017.

1036 Pérez-Estaún, A., Bea, F. and Vera, J. A.: Macizo Ibérico, Edited by: Vera, J.A., *Geología de España*,
1037 19-228, 2004.

1038 Petschick R.: [http://www.geol-pal.uni-frankfurt.de/](http://www.geol-pal.uni-frankfurt.de/Staff/Homepages/Petschick/classicsoftware.html#MacDiff)
1039 [Staff/Homepages/Petschick/classicsoftware.html#](http://www.geol-pal.uni-frankfurt.de/Staff/Homepages/Petschick/classicsoftware.html#MacDiff) MacDiff, 2004.

1040 Platt, J. P.: Dynamics of orogenic wedges and the uplift of high-pressure metamorphic rocks,
1041 *Geological Society of America Bulletin*, 97(9), 1037-1053, 1986.

- 1042 Ponce, C., Simancas, J.F., Azor, A., Martínez Poyatos, D.J., Booth-Rea, G., and Expósito, I.:
1043 Metamorphism and kinematics of the early deformation in the Variscan suture of SW Iberia,
1044 *Journal of Metamorphic Geology*, 30(7), 625-638, 2012.
- 1045 Potel, S., Ferreiro-Mählmann, R., Stern, W. B., Mullis, J., and Frey, M.: Very low-grade metamorphic
1046 evolution of pelitic rocks under high-pressure/low-temperature conditions, NW New
1047 Caledonia (SW Pacific), *Journal of Petrology*, 47(5), 991-1015, 2006
- 1048 Potel, S., Maison, T., Maillet, M., Sarr, A. C., Doublier, M. P., Trullenque, G., and Mählmann, R. F.:
1049 Reliability of very low-grade metamorphic methods to decipher basin evolution: Case study
1050 from the Markstein basin (Southern Vosges, NE France), *Applied Clay Science*, 134, 175-
1051 185, 2016.
- 1052 Quesada, C.: Geological constraints on the Paleozoic tectonic evolution of tectonostratigraphic
1053 terranes in the Iberian Massif. *Tectonophysics* 185, 225–245, 1991.
- 1054 Quesada, C.: Precambrian successions in SW Iberia: their relationship to ‘Cadomian’ orogenic events.
1055 *Geological Society, London, Special Publications*, 51(1), 353-362, 1990. Quesada, C.,
1056 Fonseca, P.E., Munhá, J., Oliveira, J.T., and Ribeiro, A.: The Beja-Acebuches Ophiolite
1057 (Southern Iberia Variscan fold belt): geological characterization and significance, *Boletín*
1058 *Geológico Minero*, 105, 3-49, 1994.
- 1059 Quesada, C., Braid, J. A., Fernandes, P., Ferreira, P., Jorge, R. S., Matos, J. X., Murphy, J.B., Oliveira,
1060 J.T., Pedro, J. and Pereira, Z.: SW Iberia Variscan Suture Zone: Oceanic Affinity Units. In
1061 *The Geology of Iberia: A Geodynamic Approach, Volume 2: The Variscan Cycle*, edited by:
1062 Quesada, C., and Oliveira, J.T., Springer. 131-171. Springer, 2019.
- 1063 Ribeiro, A., Munhá, J., Fonseca, P.E., Araujo, A., Pedro, J.C., Mateus, A., Tassinari, C., Machado, G.,
1064 and Jesus, A.: Variscan ophiolite belts in the Ossa-Morena Zone (Southwest Iberia):
1065 Geological characterization and geodynamic significance, *Gondwana Research*, 17(2-3), 408-
1066 421, 2010.
- 1067 Rubio Pascual, F.J., Matas J., and Martín Parra, L.M.: High-pressure metamorphism in the Early
1068 Variscan subduction complex of the SW Iberian Massif, *Tectonophysics*, 592, 187-199, 2013.
- 1069 Sassi, F.P., and Scolari, A.: The b_0 value of the potassic white micas as a barometric indicator in low-
1070 grade metamorphism of pelitic schists, *Contributions to Mineralogy and Petrology*, 45(2),
1071 143-152, 1974.
- 1072 Silva, J. B., Oliveira, J.T., and Ribeiro, A.: South Portuguese Zone, structural outline, in: *Pre-Mesozoic*
1073 *Geology of Iberia*, edited by: Dallmeyer, R.D., and Martínez García, E., Springer, Berlin,
1074 Germany, pp. 348-362, 1990.
- 1075 Simancas, J.F., Carbonell, R., Lodeiro, F.G., Pérez-Estaún, A., Juhlin, C., Ayarza, P., Kashubin, A.,
1076 Azor, A., Martínez Poyatos, D., Almodóvar, G.R., Pascual, E., Sáez, R., and Expósito, I.:
1077 Crustal structure of the transpressional Variscan orogen of SW Iberia: SW Iberia deep
1078 seismic reflection profile (IBERSEIS), *Tectonics*, 22(6), 1062, 2003.
- 1079 Simancas, J.F., Expósito, I., Azor, A., Martínez Poyatos, D., and González Lodeiro, F.: From the
1080 Cadomian orogenesis to the Early Palaeozoic Variscan rifting in Southwest Iberia, *Journal*
1081 *of Iberian Geology*, 30, 53-71, 2004.
- 1082 Simancas, J.F., Carbonell, R., González Lodeiro, F., Pérez-Estaún, A., Juhlin, C., Ayarza, P.,
1083 Kashubin, A., Azor A., Martínez Poyatos, D.J., Sáez, R., Almodóvar, G.R., Pascual R.,
1084 Flecha, I., and Martí, D.: Transpressional collision tectonics and mantle plume dynamics:
1085 The Variscides of southwestern Iberia, *Memoirs, Geol. Soc.*, 32(1), 345-354, 2006.

- 1086 Vázquez, M., Abad, I., Jiménez-Millán, J., Rocha, F.T., Fonseca, P.E., and Chaminé, H.I.: Prograde
1087 epizonal clay mineral assemblages and retrograde alteration in tectonic basins controlled by
1088 major strike-slip zones (W Iberian Variscan chain), *Clay Minerals*, 42(1), 109-128, 2007.
- 1089 Vidal, O., Parra, T., and Vieillard, P.: Thermodynamic properties of the Tschermak solid solution in
1090 Fe-chlorite: application to natural examples and possible role of oxidation, *American*
1091 *Mineralogist*, 90, 347-358, 2005.
- 1092 Vidal, O., de Andrade, V., Lewin, E., Muñoz, M., Parra, T., and Pascarelli, S.: P-T-deformation-
1093 Fe³⁺/Fe²⁺ mapping at the thin section scale and comparison with XANES mapping.
1094 Application to a garnet-bearing metapelite from the Sambagawa metamorphic belt (Japan),
1095 *Journal of Metamorphic Geology*, 24, 669-683, 2006.
- 1096 Vidal, O., Lanari, P., Munoz, M., Bourdelle, F., and De Andrade, V.: Deciphering temperature,
1097 pressure and oxygen-activity conditions of chlorite formation, *Clay Minerals*, 51(4), 615-633,
1098 2016.
- 1099 Warr, L.N., and Ferreiro Mählmann, R.: Recommendations for Kübler Index standardization, *Clay*
1100 *Minerals*, 50(3), 283-286, 2015.
- 1101 Warr, L.N., and Rice, A.H.N.: Inter-laboratory standardization and calibration of clay mineral
1102 crystallinity and crystallite size data, *Journal of Metamorphic Geology*, 12, 141–152, 1994.
- 1103 Whitney, D.L., and Evans, B.W.: Abbreviations for names of rock-forming minerals, *American*
1104 *mineralogist*, 95(1), 185, 2010.

Figure 1

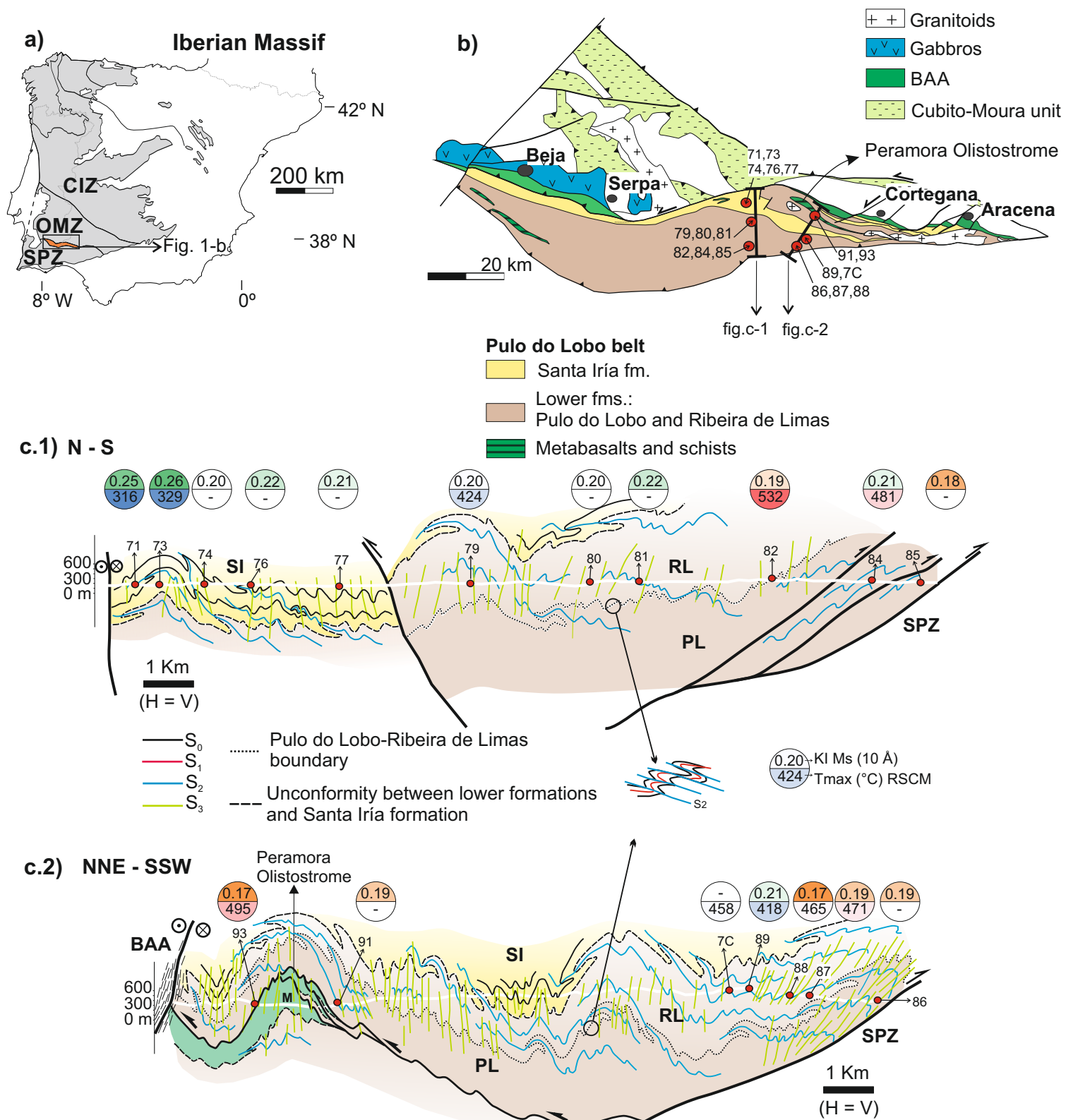


Figure 2

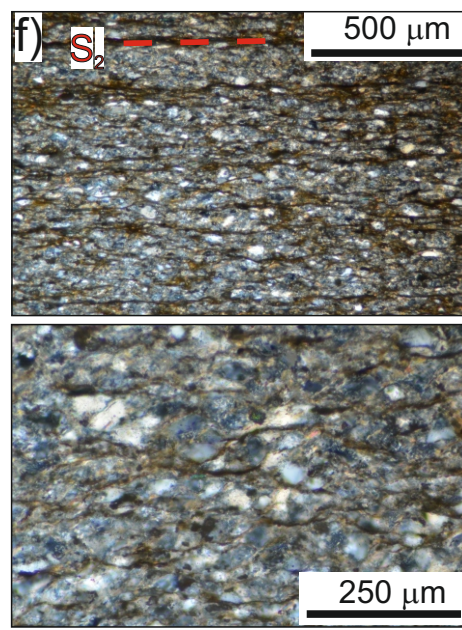
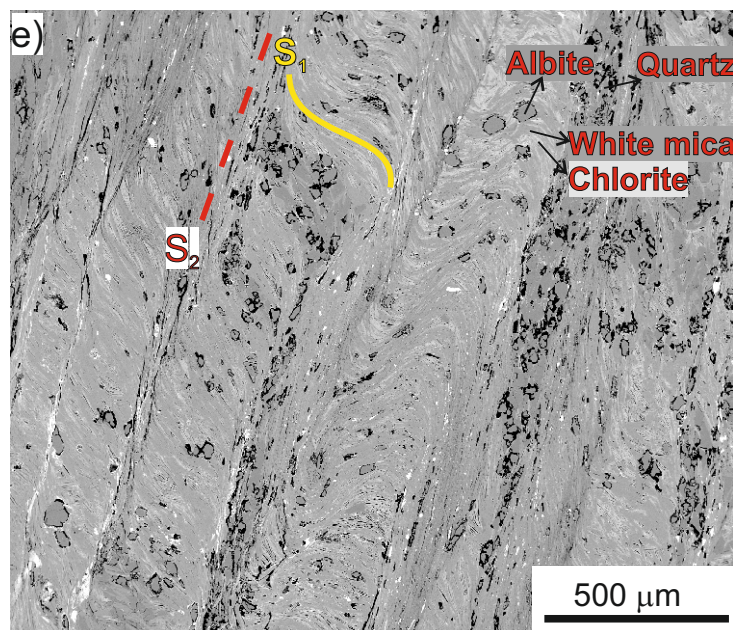
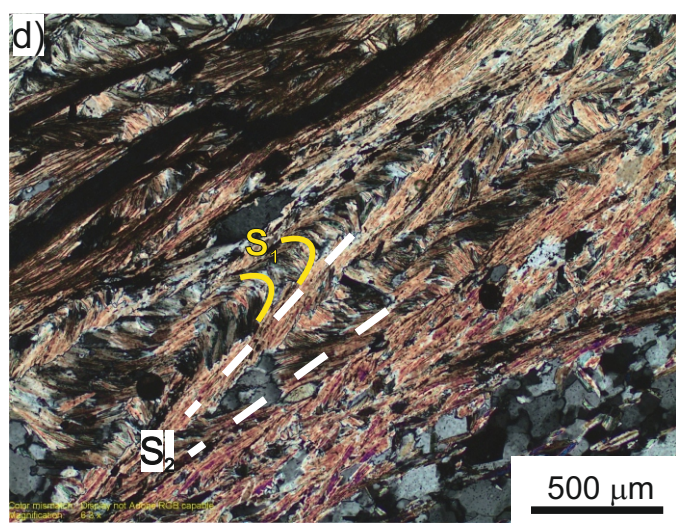
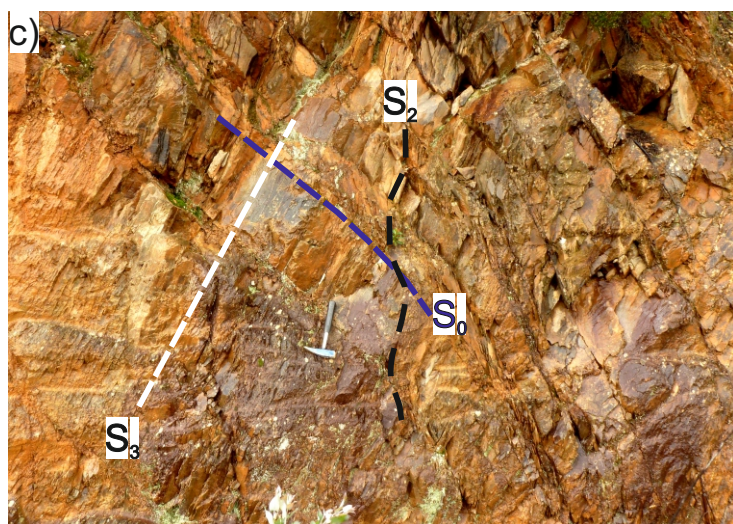
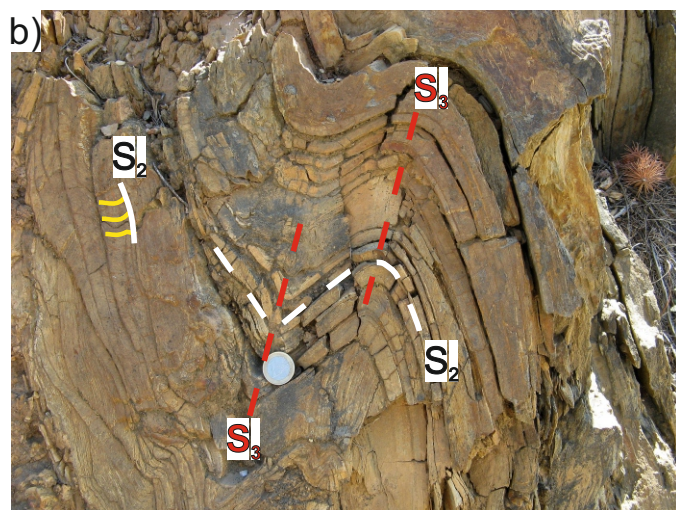
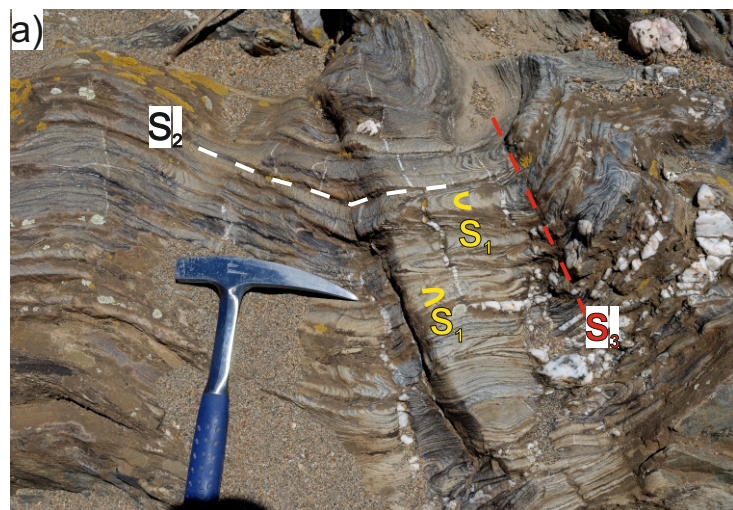


Figure 3

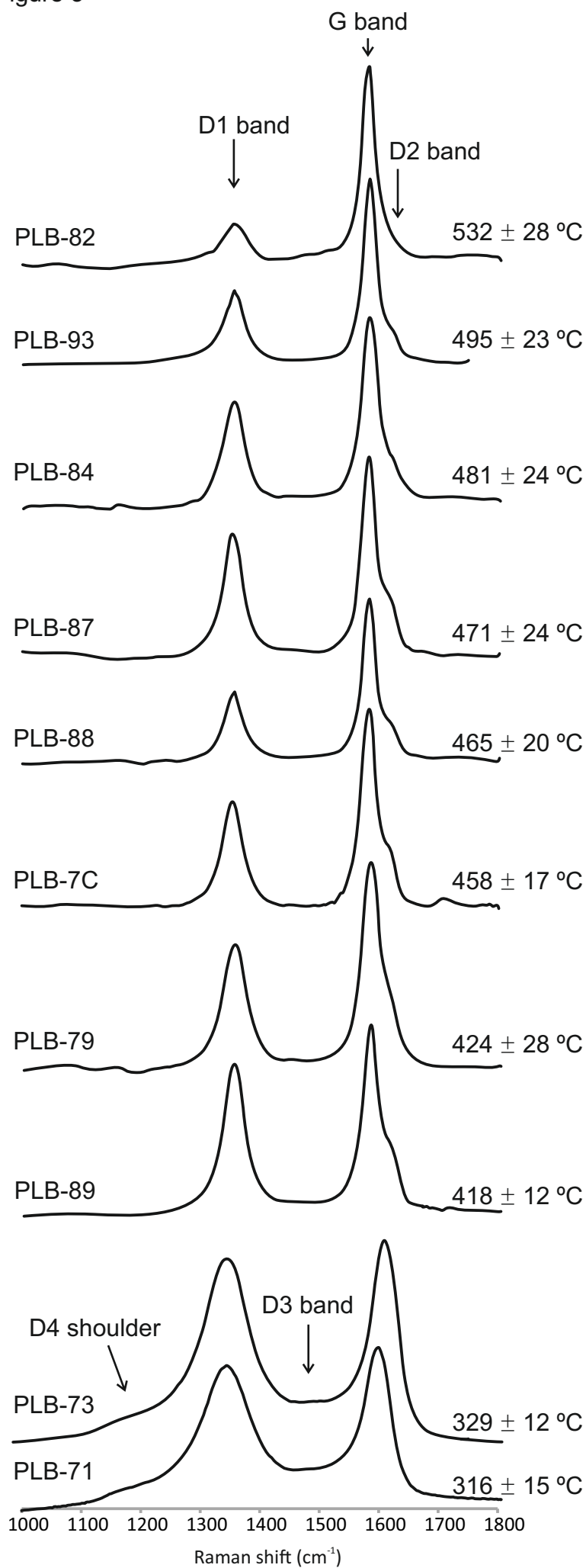


Figure 4

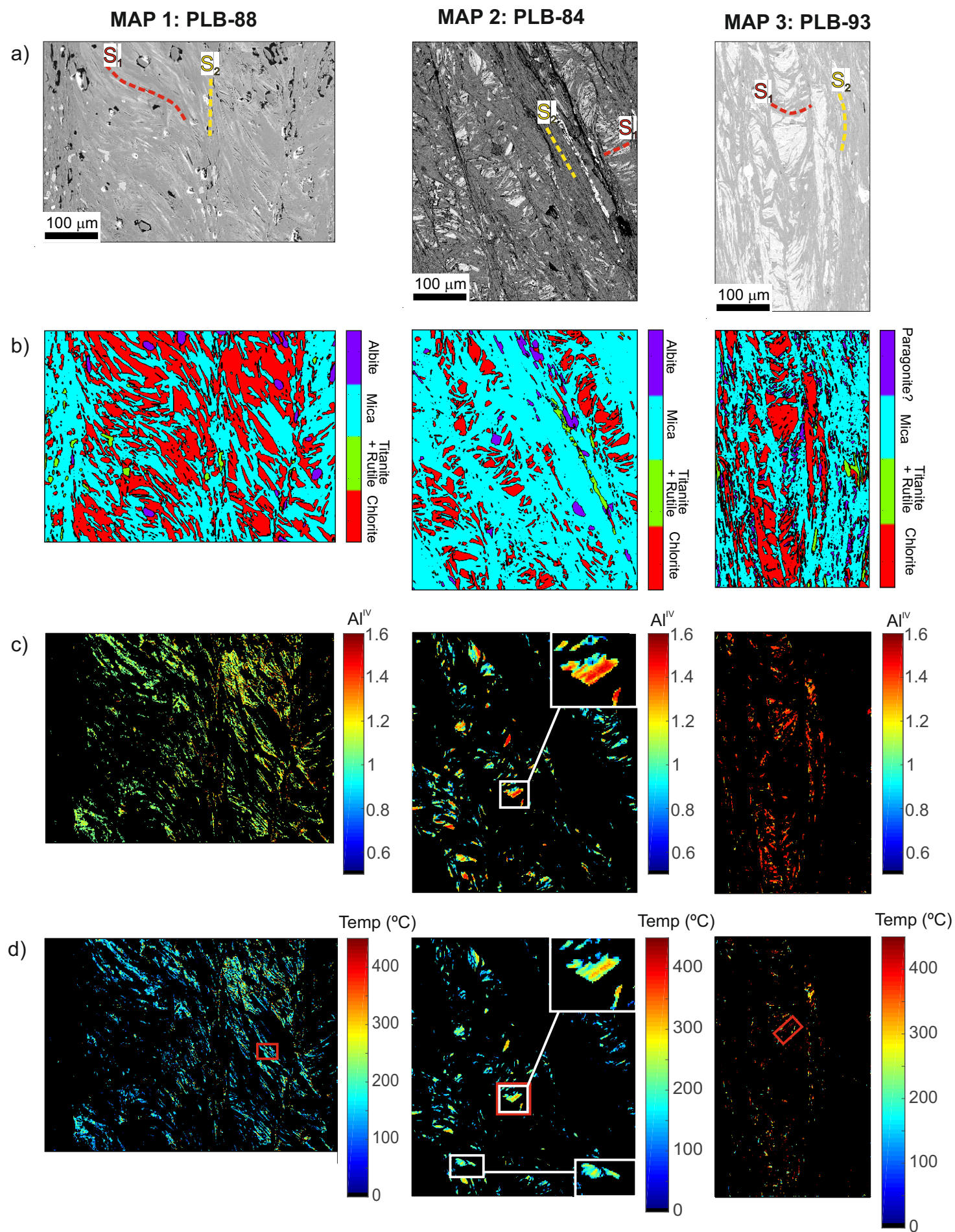


Figure 5

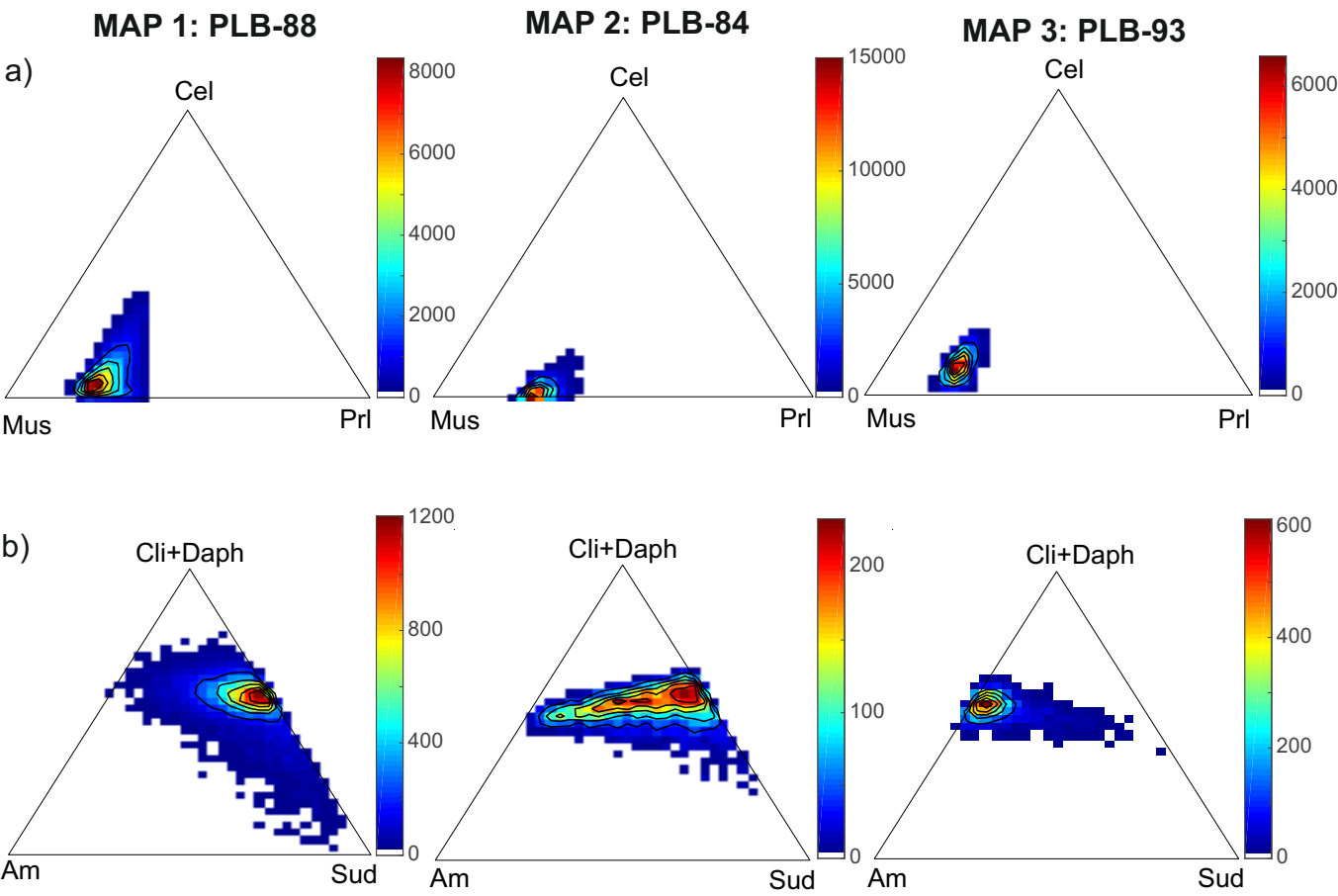


Figure 6

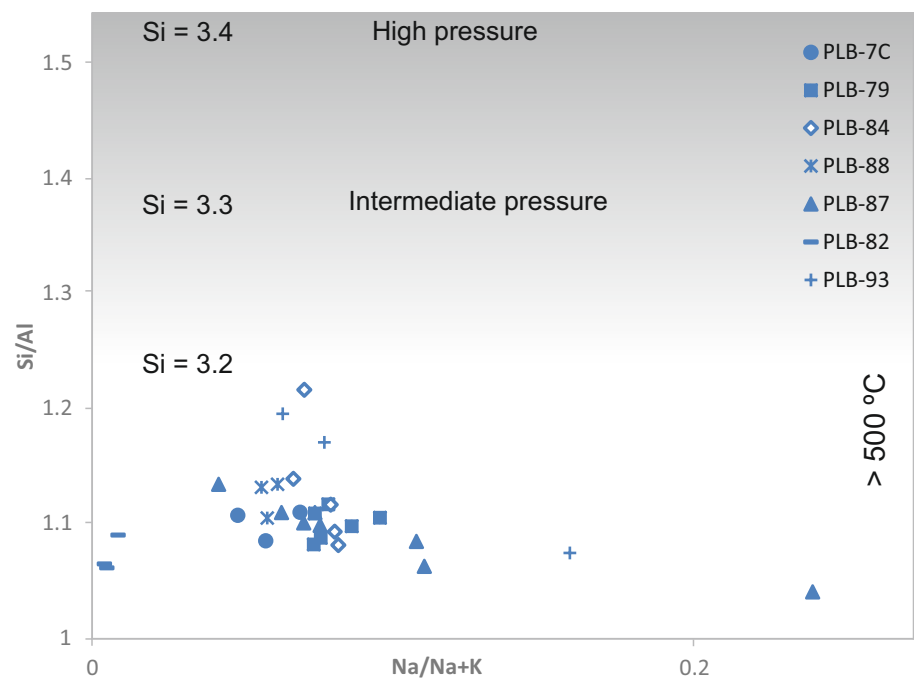
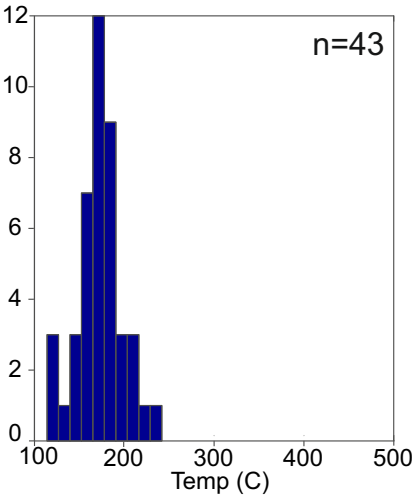
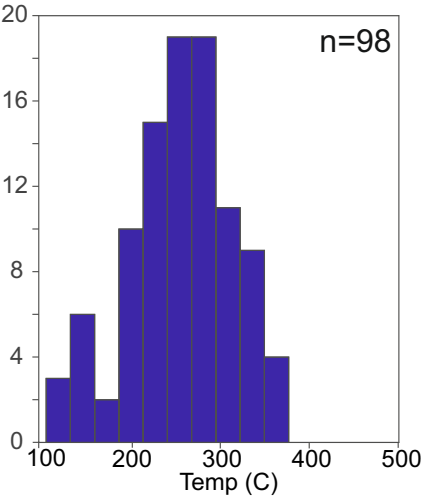


Figure 7

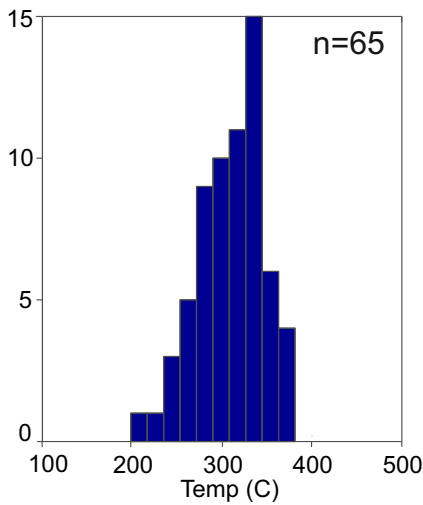
a) MAP 1: PLB-88



MAP 2: PLB-84



MAP 3: PLB-93



b)

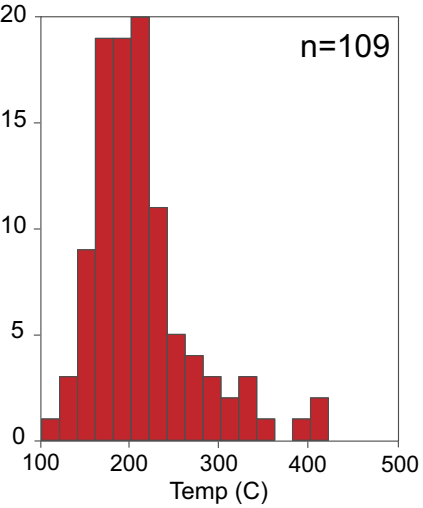
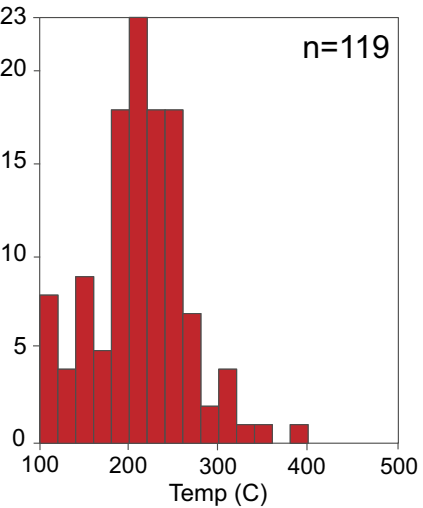
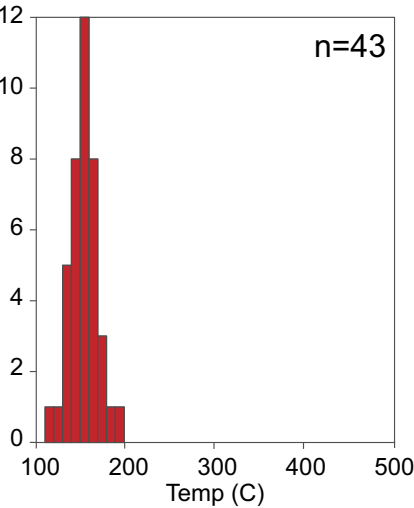


Table 1

Formation	Sample	Mineralogy	FWHM	Basel KI (10 Å)		b (Å)	d ₀₀₁ (Å)	White mica compositions			Chlorite compositions			Chlorite maps	Chlorite thermometry		T _{max} (°C) RSCM	
														(Lanari et al., 2014b)	Vidal et al., 2006	Bourdelle et al., 2013		
	PLB-	Qz + Ms + Fsp+	Å	bulk fraction	<2 µm	Ms	Ms	% Ms	% Cel	% Pri	% Cli+Daph	% Am	% Sud	T (°C)	T (°C)	T (°C)	Mean	Std Dv
Santa Iria (upper formation)	71	Chl	0.221	0.23	0.25	8.991	9.995	-			-			-	-	-	316	15
	73	Chl	0.227	0.22	0.26	8.996	9.997	-			-			-	-	-	329	12
	74	Chl + C/S	0.164	0.20	0.20	8.999	10.001	-			-			-	-	-	-	
	76	Chl	0.184	0.20	0.22	8.997	9.997	-			-			-	-	-	-	
	77	Chl + C/S	0.171	0.19	0.21	8.998	9.995	-			-			-	-	-	-	
lower fomations	79	Chl + Pg	0.17	0.18	0.20	8.995	9.993	-			-			-	-	-	424	28
	80	Chl	0.169	0.18	0.20	9.001	9.988	-			-			-	-	-	-	
	81	Chl + Pg + C/S	0.181	0.19	0.22	-	9.988	-			-			-	-	-	-	
	82	Chl + Pg	0.158	0.17	0.19	8.995	9.986	-			-			-	-	-	532	28
	84 (map 2)	Chl + Pg + C/S	0.173	0.17	0.21	8.994	9.988	70-80	0-10	20-30	50	0-50	0-50	150-350	150-375	150-350	481	24
	85	Chl + Pg	0.137	0.17	0.18	8.996	9.996	-			-			-	-	-	-	
	86	Pg + C/S	0.144	0.18	0.19	8.993	9.986	-			-			-	-	-	-	
	87	Chl + Pg	0.144	0.18	0.19	8.998	9.986	-			-			-	-	-	471	24
	88 (map 1)	Chl + Pg	0.129	0.18	0.17	8.997	9.990	70-80	0-10	20-30	50	0-10	20-50	100-200	120-230	150-200	465	20
	89	Chl	0.178	0.19	0.21	8.996	9.993	-			-			-	-	-	418	12
	91	Chl + Pg	0.143	0.17	0.19	9.000	9.995	-			-			-	-	-	-	
	93 (map 3)	Chl + Pg	0.128	0.18	0.17	9.002	9.990	70-80	0-10	20-30	50	40-50	0-10	200-450	200-380	150-400	495	23
	7C	-	-	-	-	8.993	-	-			-			-	-	-	458	17

Table 2

Time	Deformation/metamorphic phase	Temperature	Low-grade metamorphic conditions
Middle-Upper Carboniferous	S ₃ S ₂ -M ₂	- <300 °C	- Epizone-Anchizone limit
Early Carboniferous (~340 Ma)	Beja-Acebuches and Pulo do Lobo metamafigs Thermal imprint		
Upper Devonian	S ₁ -M ₁	~300-450 °C	Epizone